

# Hunger enhances food-odour attraction through a neuropeptide Y spotlight

<https://doi.org/10.1038/s41586-021-03299-4>

Nao Horio<sup>1</sup> & Stephen D. Liberles<sup>1</sup>✉

Received: 1 July 2019

Accepted: 26 January 2021

Published online: 3 March 2021

 Check for updates

Internal state controls olfaction through poorly understood mechanisms. Odours that represent food, mates, competitors and predators activate parallel neural circuits that may be flexibly shaped by physiological need to alter behavioural outcome<sup>1</sup>. Here we identify a neuronal mechanism by which hunger selectively promotes attraction to food odours over other olfactory cues. Optogenetic activation of hypothalamic agouti-related peptide (AGRP) neurons enhances attraction to food odours but not to pheromones, and branch-specific activation and inhibition reveal a key role for projections to the paraventricular thalamus. Mice that lack neuropeptide Y (NPY) or NPY receptor type 5 (NPY5R) fail to prefer food odours over pheromones after fasting, and hunger-dependent food-odour attraction is restored by cell-specific NPY rescue in AGRP neurons. Furthermore, acute NPY injection immediately rescues food-odour preference without additional training, indicating that NPY is required for reading olfactory circuits during behavioural expression rather than writing olfactory circuits during odour learning. Together, these findings show that food-odour-responsive neurons comprise an olfactory subcircuit that listens to hunger state through thalamic NPY release, and more generally, provide mechanistic insights into how internal state regulates behaviour.

The mouse olfactory system elicits myriad behaviours that include feeding, mating, fighting and predator escape. The choice of behavioural action is strongly influenced by physiological need; however, mechanisms by which internal state shapes olfactory circuits remain poorly defined. Hunger is a powerful motivational state that intensely drives behaviours that are predictive of food consumption<sup>2,3</sup>. In humans, hunger enhances the pleasantness rating of food odours<sup>4</sup>, whereas in mice, starvation affects general features of olfaction, such as arousal, sniffing rate and sensitivity to novel odours<sup>5</sup>. Here we asked whether and how hunger might exert selective control over olfactory subcircuits that attend to food odours.

Various odours activate discrete neuronal ensembles in the olfactory epithelium, olfactory bulb and olfactory cortex<sup>1</sup>. In the mouse, both food odours and volatile sex pheromones are attractive<sup>1</sup> but are relevant for different physiological drives, which suggests that responsive neurons at some circuitry node display key differences, such as in connectivity, gene expression and/or hormone responsiveness. Hunger-dependent modulation of olfactory inputs has been proposed to occur early in olfactory processing in vertebrates<sup>5–7</sup> and in other model organisms<sup>8</sup>. Satiety state alters the hedonic quality of food, but is not thought to affect the ability to recognize or detect food, which would be maladaptive for locating food stores for future use<sup>4</sup>. It is therefore also possible that behaviourally relevant state-dependent modulation occurs through central pathways that are downstream of primary olfactory areas.

## Hunger state guides odour responses

We used a simple and robust two-choice assay to investigate hunger-dependent odour responses. Mice were placed in a test arena containing

volatile odour ports on each side without direct stimulus contact<sup>9</sup> (Fig. 1a). Investigation time was quantified as the time in which the nose of the mouse was directly above an odour port, and a preference index was calculated as the normalized difference in odour investigation times. Mice were attracted to both food odours (familiar home-cage chow dissolved in water and centrifuged to remove insoluble debris) and pheromones (urine of opposite-sex mice) compared with water (Extended Data Fig. 1). When paired against each other, food odours and pheromones were similarly attractive to fed mice. By contrast, fasted mice (both male and female) displayed a strong preference for food odours over pheromones; hunger was found to promote food-odour investigation in two-choice comparisons or in single-odour pairings with water (Fig. 1b, Extended Data Fig. 1). Conversely, previous exposure to a mate increased attraction to volatile pheromones over food odours in fed but not in fasted mice (Extended Data Fig. 2), which is consistent with need-based prioritization of behaviour<sup>10</sup>. The observation that hunger enhances attraction to food odours relative to pheromones suggests that specific olfactory subcircuits can be differentially modulated by hunger-control centres in the brain.

## A hypothalamus-to-thalamus circuit

Hypothalamic neurons expressing AGRP help to generate hunger drive. Optogenetic and chemogenetic activation of AGRP neurons in the arcuate nucleus powerfully motivates feeding behaviour<sup>11,12</sup>, whereas ablation of AGRP neurons in adult mice causes lethal starvation<sup>13</sup>. We therefore asked whether optogenetic activation of hypothalamic AGRP neurons alters odour-preference behaviour (Fig. 1c–e, Extended Data Fig. 3a–c). Optogenetic activation was achieved in *Agrp-ires-cre* mice

<sup>1</sup>Howard Hughes Medical Institute, Department of Cell Biology, Harvard Medical School, Boston, MA, USA. ✉e-mail: Stephen\_Liberles@hms.harvard.edu

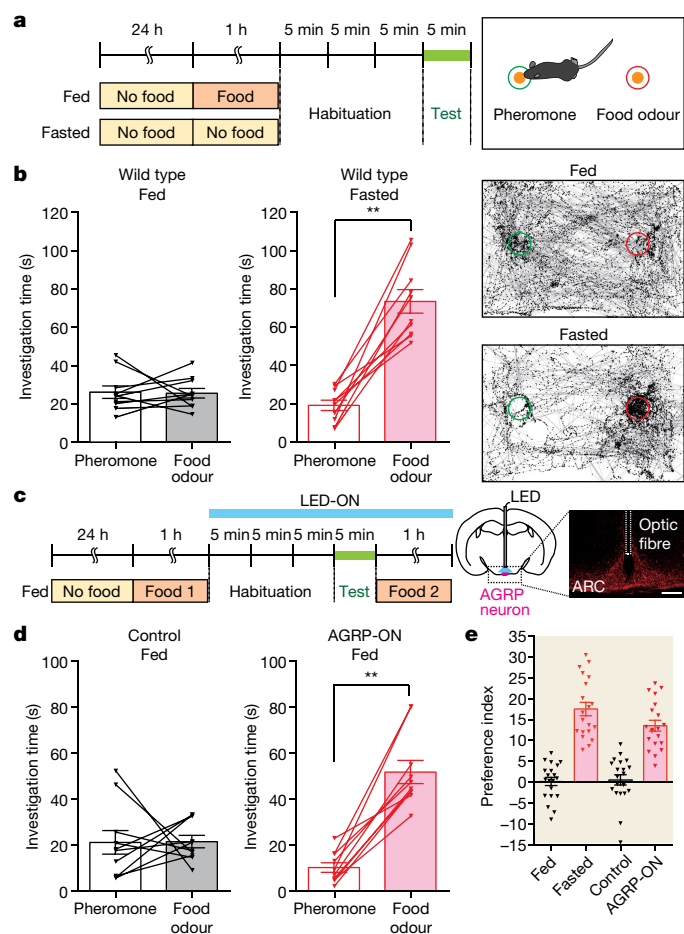


**Fig. 1 | Hunger and AGRP neuron activation promote attraction to food odours over pheromones.** **a**, Timeline (left) and schematic (right) of the two-choice behavioural assay. **b**, Left, investigation times of fed and fasted male wild-type mice to pheromones and food odours. Right, behaviour of representative mice, in which nose position is traced (black) over the 5-min trial. **c**, Timeline (left) of the two-choice assay involving AGRP neuron optogenetics, with the location of the optic fibre depicted in a schematic (right) based on published brain section images<sup>31</sup>. Scale bar, 200  $\mu$ m. **d**, Investigation times of fed control and fed AGRP-ON male mice to pheromones and food odours. **e**, Preference indices for food odours over pheromones in the indicated mice.  $n = 10$  mice, except **e** for which  $n = 10$  males and 10 females. Data are mean  $\pm$  s.e.m., lines with triangles represent individual mice.  $^{**}P < 0.01$ , two-tailed Wilcoxon test.

containing a channelrhodopsin reporter allele (*lsl-ChR2*) using optic fibres implanted in the arcuate nucleus. Light stimulation in fed control mice (*AgRP-ires-cre*) did not alter odour-preference behaviour, but in fed AGRP-ON mice (*AgRP-ires-cre;lsl-ChR2*) light stimulation strongly enhanced behavioural attraction to food odours relative to pheromones, with a preference similar to that of fasted wild-type mice. Thus, AGRP neurons promote behavioural attraction through some olfactory pathways but not others.

Next, we asked whether AGRP neuron terminals in specific brain regions promote attraction to food odours (Fig. 2a). Collectively, AGRP neurons have widespread projections, and approaches that involve terminal-specific optogenetics in AGRP neurons have revealed a marked division of labour among downstream targets<sup>14–17</sup>. Individual AGRP neurons can display selectivity among target areas, so branch-specific illumination does not cause anti-dromic activation of axon terminals in all other locations<sup>15</sup>. *AgRP-ires-cre* (AGRP-ON) or wild-type (control) mice were injected with a Cre-dependent adeno-associated virus (AAV) encoding channelrhodopsin (*AAV-DIO-ChR2*) in the arcuate nucleus,

and optic fibres were used to illuminate various brain areas that receive input from AGRP neurons. Optogenetic stimulation of AGRP neuron terminals in the paraventricular thalamus (PVT), but not in other brain regions analysed, promoted food-odour attraction in fed AGRP-ON mice (Fig. 2b, Extended Data Fig. 3d, e); similar responses were seen in mice that were re-fed acutely after a fast or were fed ad libitum (Extended Data Fig. 3f–h). Responses were of similar magnitude after somatic stimulation of AGRP neurons and were not observed in control mice that lacked Cre (Fig. 2b). Optogenetic activation of AGRP terminals in other brain regions failed to induce food-odour preference in fed mice (Fig. 2b, Extended Data Fig. 3d), including the bed nucleus of the stria terminalis (BNST), the paraventricular hypothalamus (PVH), the central nucleus of the amygdala (CeA), the lateral hypothalamus (LH), the medial amygdala (MeA), the periaqueductal grey (PAG) and the parabrachial nucleus (PBN). Notably, stimulating AGRP axons in the BNST, the PVH and the LH promoted robust food consumption in fed mice (Fig. 2c)—as has been reported previously<sup>15</sup>—but did not enhance food-odour preference. Moreover, AGRP neurons that target the MeA and the PBN suppress competing behaviours that are related to aggression and pain<sup>14,17</sup>, but were also not involved in odour preference.

Food-odour perception can arise from experience, so we next asked whether novel odours could be entrained as food odours and subsequently evoke state-dependent responses (Extended Data Fig. 4). Food-restricted mice were given a diet of strawberry gelatin during a four-day training period. Before training, mice preferred pheromone odour to strawberry-gelatin odour whether fed or fasted; however, after training, mice displayed hunger-dependent attraction to strawberry-gelatin odour. Furthermore, optogenetic stimulation of AGRP neuron terminals in the PVT promoted attraction to strawberry-gelatin odour only after training.

Because the stimulation of AGRP neuron projections to the PVT promoted food-odour attraction in fed mice, we asked whether silencing these projections decreased food-odour attraction in fasted mice. The expression of an inhibitory opsin, halorhodopsin, in AGRP neurons caused light-induced reductions in membrane potential and firing rate (Extended Data Fig. 5a). We inserted optic fibres in the PVT (PVT-OFF) or in the arcuate nucleus (ARC-OFF) of *AgRP-ires-cre;lsl-halorhodopsin* mice or in control *AgRP-ires-cre* mice. Illumination of these fibres in fasted PVT-OFF or ARC-OFF mice, but not in control mice that lacked halorhodopsin, decreased food-odour attraction to levels seen in fed mice (Fig. 2d, Extended Data Fig. 5b, c); these findings indicate that AGRP neuron projections to the PVT are required for hunger-dependent enhancement of food-odour attraction. Despite similar odour-preference responses, post-assay feeding was normal in fasted PVT-OFF mice but was reduced in fasted ARC-OFF mice (Extended Data Fig. 5d). The PVT is located dorsally within the thalamus, and notably, in humans, attention to food odours engages the dorsal thalamus and the amygdala<sup>18</sup>; moreover, patients with lesions in the dorsal thalamus perceive food odours as neutral or aversive without losing the ability to identify them<sup>19</sup>.

AGRP neurons display transient decreases in activity when food cues are presented<sup>20,21</sup>. We used fibre photometry to investigate whether similar changes were observed in PVT-projecting AGRP axons. We injected the arcuate nucleus of *AgRP-ires-cre* mice with an AAV containing a Cre-dependent *GCaMP6s* allele, placed optic fibres in the arcuate nucleus, the PVT or the PVH, and recorded responses in fasted mice presented with food odours or pheromones (Extended Data Fig. 6). Food odour transiently inhibited the activity of AGRP neurons in all locations measured, whereas pheromones had no effect. Notably, decreases in AGRP neuron activity were short-lived, whereas attraction to food odours persisted throughout the behavioural assay. Moreover, optogenetic stimulation—not inhibition—of AGRP neurons promoted food-odour attraction, whereas optogenetic inhibition of AGRP neurons, which was sustained for longer than the transient decreases in activity observed during food-odour presentation, blocked fasting-induced attraction

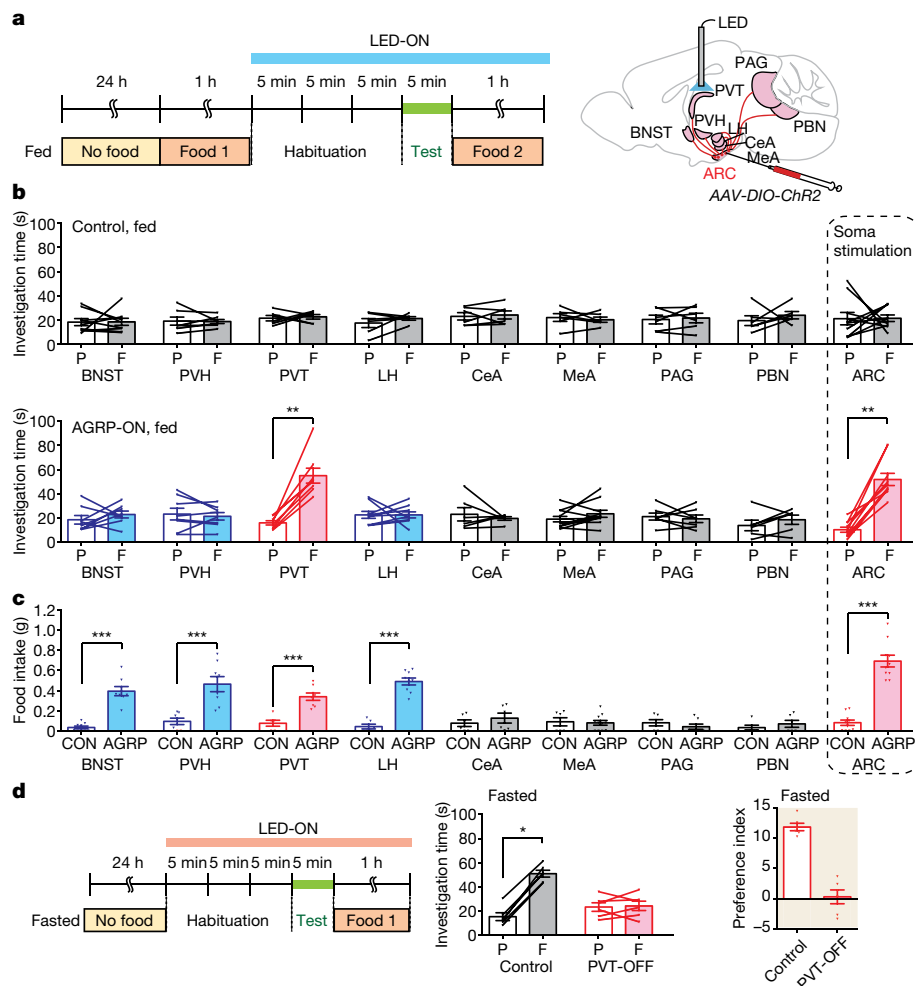


**Fig. 2 | Thalamic AGRP neuron projections promote food-odour attraction.**

**a**, Timeline (left) of two-choice assay involving optogenetic stimulation of AGRP neurons (blue bar), with the location of the optic fibre depicted in a schematic (right) based on published brain section images<sup>31</sup>. **b**, Investigation times of fed control (top) and fed AGRP-ON (bottom) mice to pheromones (P) and food odours (F) after optogenetic stimulation of AGRP axon terminals in the indicated brain regions. **c**, Food consumption after the two-choice odour test ('Food 2' in the timeline in **a**) in fed control (CON) and fed AGRP-ON

(AGRP) mice after illumination of the indicated brain regions. **d**, Timeline (left), investigation times (middle) and preference indices (right) of optogenetic inhibition experiments involving illumination of the PVT. *n* (number of mice used for control, AGRP-ON in **b**, **c**) = BNST: 9, 8; PVH: 7, 8; PVT: 6, 8; LH: 6, 9; CeA: 6, 6; MeA: 6, 11; PAG: 6, 7; PBN: 6, 6; ARC: 10, 10. *n* (in **d**) = 6 mice. Male and female mice were used. Data are mean  $\pm$  s.e.m., lines with triangles represent individual mice, \**P* < 0.05, \*\**P* < 0.01, \*\*\**P* < 0.001, two-tailed Wilcoxon test (except for **c**, two-tailed Mann–Whitney *U*-test).

to food odours. We propose that the persistent stimulation of AGRP neurons that occurs during a fasted state enhances food-odour attraction through sustained signalling in downstream neurons, perhaps through the durable action of a neuromodulator.

### Roles for NPY and its receptor NPY5R

We next asked whether any of the three principal neurotransmitters released by AGRP neurons—AGRP, NPY or GABA ( $\gamma$ -aminobutyric acid)<sup>22</sup>—were required for hunger-dependent odour attraction (Fig. 3a, b, Extended Data Fig. 7a–c). We obtained knockout mice that lacked GABA (*Agrp-ires-cre;Vgat-flox*, or *GABA-KO*), NPY (*Npy-KO*), or melanocortin receptor 4 (*Mcr4-KO*)—a receptor that mediates key physiological effects of hypothalamic AGRP. Notably, fasted *Npy-KO* mice did not prefer food odour over pheromones, whereas fasted *GABA-KO* and *Mcr4-KO* mice displayed normal hunger-dependent food-odour attraction. When fed, attraction to food odours and pheromones was similar in *GABA-KO*, *Npy-KO*, *Mcr4-KO* and wild-type mice. Fed *Npy-KO* mice therefore retain a lower level of attraction to food odours that is comparable to their attraction to pheromones, but they show no hunger-dependent

enhancement of food-odour preference. The enhancement of pheromone attraction that was observed after previous exposure to a mate persisted in *Npy-KO* mice (Extended Data Fig. 2), which suggests that other mechanisms—independent of NPY—are involved in toggling pheromone-responsive olfactory circuits.

NPY is expressed in many neuron types, including AGRP neurons. We performed cell-specific NPY rescue to determine whether the behavioural deficits that were observed in global *Npy-KO* mice were due to the loss of NPY expression in AGRP neurons<sup>23</sup>. A Cre-dependent AAV encoding NPY (*AAV-DIO-Npy*) was injected into the arcuate nucleus of *Agrp-ires-cre;Npy-KO* (*Npy*<sup>AGRP</sup> rescue) or *Npy-KO* (control) mice. The rescue of NPY expression in AGRP neurons restored hunger-dependent food-odour attraction (Fig. 3c, d, Extended Data Fig. 7d), which indicates that AGRP-neuron-derived NPY is sufficient for state-dependent modulation of food-odour responses.

NPY receptors comprise a small subfamily of five G-protein-coupled receptors. To determine whether a particular NPY receptor was responsible for the observations described here, we obtained knockout mice that lacked individual NPY receptors and tested their odour preferences (Fig. 3e, f, Extended Data Fig. 7e–g). Fasted male and female *Npy5r-KO*

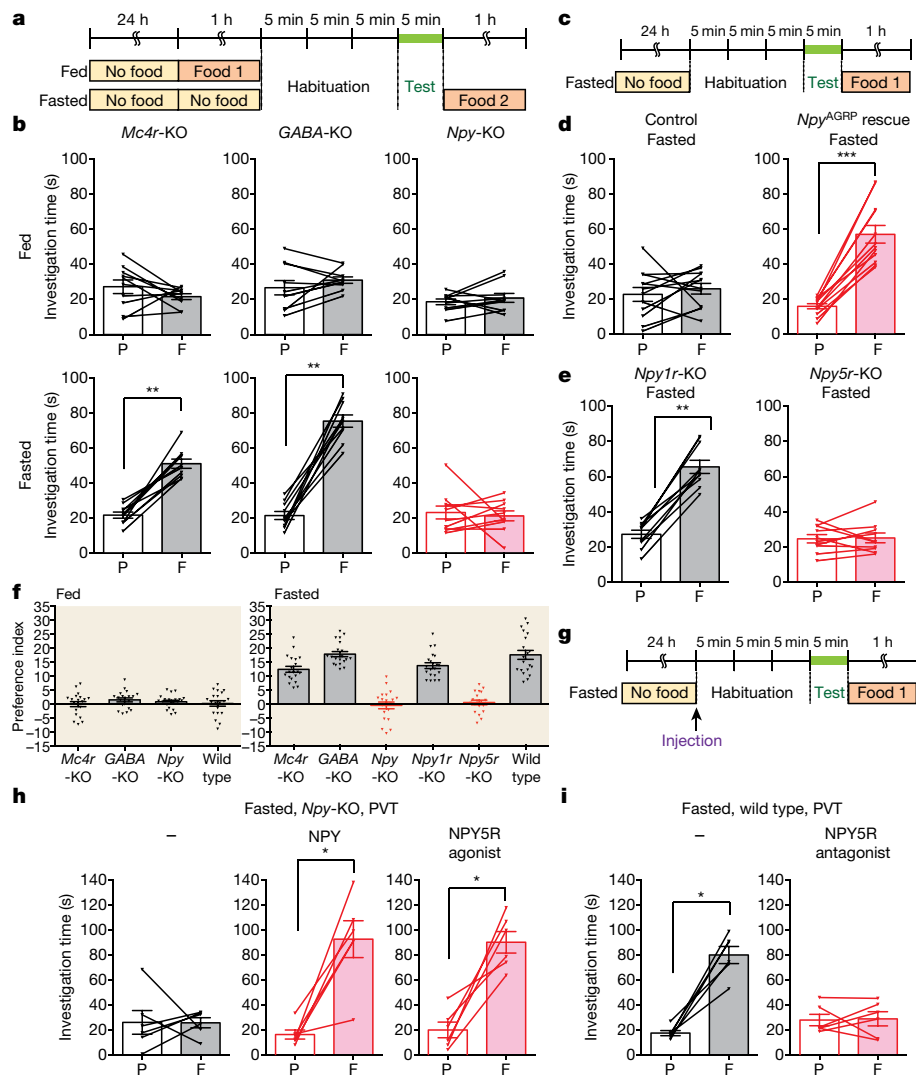


**Fig. 3 | NPY and NPY5R are required for hunger-dependent food-odour attraction.** **a, b**, Timeline (**a**) and odour investigation times (**b**) in fed and fasted male mice indicated.  $n = 10$  mice per group. Data are mean  $\pm$  s.e.m., lines with triangles represent individual mice. **c, d**, Timeline (**c**) and odour investigation times (**d**) in *Npy*-KO (control) and *Agrp-ires-cre;Npy-KO* (*Npy*<sup>AGRP</sup> rescue) mice three weeks after injection of *AAV-DIO-Npy* in the arcuate nucleus.  $n = 12$  mice per group. Male and female mice were used. Data are mean  $\pm$  s.e.m., lines with triangles represent individual mice. **e, f**, Investigation times (**e**) and odour preference indices (**f**) for fed and fasted mice indicated.  $n = 10$  mice, except for the preference index experiments in which  $n = 10$  male and 10 female

mice. Data are mean  $\pm$  s.e.m., lines with triangles represent individual mice. **g, h**, Timeline (**g**) and odour investigation times (**h**) for fasted *Npy*-KO mice injected in the PVT with artificial cerebrospinal fluid (aCSF) alone (-), NPY (0.02 mg kg<sup>-1</sup> in aCSF) or NPY5R agonist ([ICPP<sup>1-7</sup>, NPY<sup>19-23</sup>, Ala<sup>31</sup>, Aib<sup>32</sup>, Gln<sup>34</sup>]-hPancreatic polypeptide, 0.002 mg kg<sup>-1</sup> in aCSF).  $n = 3$  male and 3 female mice. Data are mean  $\pm$  s.e.m., lines with triangles represent individual mice. **i**, Investigation times for fasted wild-type mice injected in the PVT with aCSF alone (-) or NPY5R antagonist (CGP71683, 0.2 mg kg<sup>-1</sup> in aCSF).  $n = 3$  male and 3 female mice. Data are mean  $\pm$  s.e.m., lines with triangles represent individual mice. \* $P < 0.05$ , \*\* $P < 0.01$ , \*\*\* $P < 0.001$ , two-tailed Wilcoxon test.

mice showed no preference for food odours over pheromones, despite normal hunger-dependent food consumption, whereas fasted *Npy1r*-KO mice displayed normal odour-preference behaviour. Like *Npy*-KO mice, *Npy5r*-KO mice displayed attraction to food odour over water in the fed state, but showed no hunger-dependent enhancement of this response (Extended Data Fig. 8). Hunger also promoted a search for food buried in bedding, and food-search behaviour was impaired in fasted *Npy*-KO and *Npy5r*-KO mice (Extended Data Fig. 9a). Together, these findings reveal an essential role for both a neuropeptide, NPY, and its receptor, NPY5R, in hunger-evoked odour attraction.

RNA in situ hybridization experiments revealed detectable expression of *Npy5r* in cortical regions—including in the olfactory cortex—but not in the PVT (Extended Data Fig. 9b, c). One possibility is that NPY5R is localized to incoming cortical axons that arrive in the dorsal thalamus. Injection of NPY5R antagonists into the PVT blocked food-odour

attraction in fasted mice, whereas injections of NPY5R agonists promoted food-odour attraction in *Npy*-KO mice (Fig. 3g–i, Extended Data Fig. 10a, b). Similar injections of agonist into the dorsal third ventricle—just above the PVT—had no effect on food-odour attraction; however, injecting higher concentrations of agonist into the ventral third ventricle an hour before behavioural assessment enhanced food-odour attraction, presumably because sufficient agonist could then access the PVT (Extended Data Fig. 10c, d). Together, pharmacological and optogenetic studies indicate that AGRP-neuron-derived NPY5R agonism within the PVT underlies the enhancement of food-odour attraction during hunger.

In mice, perception of food odours can arise through learning (Extended Data Fig. 4). Thus, loss of hunger-evoked food-odour preference in both *Npy*-KO and *Npy5r*-KO mice could be explained by deficits in memory formation, hunger-induced behavioural expression or



both. AGRP neurons provide a negative valence teaching signal<sup>20</sup>, and in *Drosophila*, an NPY homologue is required for appetitive memory performance<sup>24</sup>. If NPY were required for the formation of food-odour memory, then the re-administration of NPY in *Npy*-KO mice would not restore hunger-dependent food-odour preference until learning could subsequently occur. We observed that the injection of NPY, or of a specific NPY5R agonist, into fasted *Npy*-KO mice immediately restored hunger-dependent food-odour preference in the absence of additional training (Fig. 3g–i). Mice had learnt that particular olfactory cues were associated with food in the absence of NPY, which probably explains the persistent basal attraction to food odour in fed *Npy*-KO mice. NPY therefore acts in the expression of hunger-enhanced food-odour attraction rather than in the formation of food-odour memory.

## Discussion

Many pathways have been proposed by which nutrients and feeding-relevant hormones might interact with the olfactory system. Here we reveal an essential role for NPY and its receptor NPY5R in hunger-dependent odour preference. AGRP neurons that project to the PVT provide a key first connection from hunger neurons to olfactory circuits. Olfaction has been considered to be unique among the senses in that olfactory inputs largely access cortical regions without traversing the thalamus<sup>25</sup>, although a minor output pathway of the piriform cortex involves the medio-dorsal thalamic nucleus<sup>26</sup>, which is adjacent to the PVT. In addition, top-down olfactory inputs—such as from the prefrontal cortex—descend on the PVT<sup>27</sup>, where they can presumably be integrated with information about hunger state from AGRP neurons. Notably, the PVT gates information from other states, including thirst<sup>28</sup>, and from other sensory systems, including visual cues<sup>29</sup>, and may generally guide attention to salient inputs that are relevant for a current behavioural state. The PVT also has a role in withdrawal symptoms associated with drug addiction<sup>30</sup>, which is consistent with a function in enhancing the valence of environmental cues that alleviate negative stressors, such as hunger, thirst and drug craving.

Neuromodulation that controls the relative strength of signals through different sensory channels allows for flexible behaviours that vary with need. Here we uncover molecular features that are essential for one such neuromodulatory pathway, as NPY from AGRP neurons opens a thalamic hunger gate for specific olfactory inputs that carry an NPY5R encryption. It seems likely that different neurotransmitters function as spotlights for other behavioural drives, with the thalamus serving a general role as a switchboard that gates preferential attention to sensory inputs on the basis of physiological need.

## Online content

Any methods, additional references, Nature Research reporting summaries, source data, extended data, supplementary information, acknowledgements, peer review information; details of author contributions and competing interests; and statements of data and code availability are available at <https://doi.org/10.1038/s41586-021-03299-4>.

- Li, Q. & Liberles, S. D. Aversion and attraction through olfaction. *Curr. Biol.* **25**, R120–R129 (2015).
- Andermann, M. L. & Lowell, B. B. Toward a wiring diagram understanding of appetite control. *Neuron* **95**, 757–778 (2017).
- Sternson, S. M. Hypothalamic survival circuits: blueprints for purposive behaviors. *Neuron* **77**, 810–824 (2013).
- Rolls, E. T. Taste, olfactory, and food reward value processing in the brain. *Prog. Neurobiol.* **127**, 64–90 (2015).
- Tong, J. et al. Ghrelin enhances olfactory sensitivity and exploratory sniffing in rodents and humans. *J. Neurosci.* **31**, 5841–5846 (2011).
- Negroni, J. et al. Neuropeptide Y enhances olfactory mucosa responses to odorant in hungry rats. *PLoS ONE* **7**, e45266 (2012).
- Soria-Gómez, E. et al. The endocannabinoid system controls food intake via olfactory processes. *Nat. Neurosci.* **17**, 407–415 (2014).
- Root, C. M., Ko, K. I., Jafari, A. & Wang, J. W. Presynaptic facilitation by neuropeptide signaling mediates odor-driven food search. *Cell* **145**, 133–144 (2011).
- Li, Q. et al. Synchronous evolution of an odor biosynthesis pathway and behavioral response. *Curr. Biol.* **23**, 11–20 (2013).
- Burnett, C. J. et al. Need-based prioritization of behavior. *eLife* **8**, e44527 (2019).
- Aponte, Y., Atasoy, D. & Sternson, S. M. AGRP neurons are sufficient to orchestrate feeding behavior rapidly and without training. *Nat. Neurosci.* **14**, 351–355 (2011).
- Krashes, M. J. et al. Rapid, reversible activation of AgRP neurons drives feeding behavior in mice. *J. Clin. Invest.* **121**, 1424–1428 (2011).
- Luquet, S., Perez, F. A., Hnasko, T. S. & Palmiter, R. D. NPY/AgRP neurons are essential for feeding in adult mice but can be ablated in neonates. *Science* **310**, 683–685 (2005).
- Alhadeff, A. L. et al. A neural circuit for the suppression of pain by a competing need state. *Cell* **173**, 140–152.e15 (2018).
- Betley, J. N., Cao, Z. F., Ritola, K. D. & Sternson, S. M. Parallel, redundant circuit organization for homeostatic control of feeding behavior. *Cell* **155**, 1337–1350 (2013).
- Essner, R. A. et al. AgRP neurons can increase food intake during conditions of appetite suppression and inhibit anorexigenic parabrachial neurons. *J. Neurosci.* **37**, 8678–8687 (2017).
- Padilla, S. L. et al. Agouti-related peptide neural circuits mediate adaptive behaviors in the starved state. *Nat. Neurosci.* **19**, 734–741 (2016).
- Small, D. M., Veldhuizen, M. G., Felsted, J., Mak, Y. E. & McGlone, F. Separable substrates for anticipatory and consummatory food chemosensation. *Neuron* **57**, 786–797 (2008).
- Rousseaux, M., Muller, P., Gahide, I., Mottin, Y. & Romon, M. Disorders of smell, taste, and food intake in a patient with a dorsomedial thalamic infarct. *Stroke* **27**, 2328–2330 (1996).
- Betley, J. N. et al. Neurons for hunger and thirst transmit a negative-valence teaching signal. *Nature* **521**, 180–185 (2015).
- Chen, Y., Lin, Y. C., Kuo, T. W. & Knight, Z. A. Sensory detection of food rapidly modulates arcuate feeding circuits. *Cell* **160**, 829–841 (2015).
- Krashes, M. J., Shah, B. P., Koda, S. & Lowell, B. B. Rapid versus delayed stimulation of feeding by the endogenously released AgRP neuron mediators GABA, NPY, and AgRP. *Cell Metab.* **18**, 588–595 (2013).
- Chen, Y. et al. Sustained NPY signaling enables AgRP neurons to drive feeding. *eLife* **8**, e46348 (2019).
- Krashes, M. J. et al. A neural circuit mechanism integrating motivational state with memory expression in *Drosophila*. *Cell* **139**, 416–427 (2009).
- Kay, L. M. & Sherman, S. M. An argument for an olfactory thalamus. *Trends Neurosci.* **30**, 47–53 (2007).
- Tham, W. W., Stevenson, R. J. & Miller, L. A. The functional role of the medio dorsal thalamic nucleus in olfaction. *Brain Res. Rev.* **62**, 109–126 (2009).
- Otis, J. M. et al. Paraventricular thalamus projection neurons integrate cortical and hypothalamic signals for cue-reward processing. *Neuron* **103**, 423–431 (2019).
- Zhu, Y. et al. Dynamic salience processing in paraventricular thalamus gates associative learning. *Science* **362**, 423–429 (2018).
- Livneh, Y. et al. Homeostatic circuits selectively gate food cue responses in insular cortex. *Nature* **546**, 611–616 (2017).
- Kirouac, G. J. Placing the paraventricular nucleus of the thalamus within the brain circuits that control behavior. *Neurosci. Biobehav. Rev.* **56**, 315–329 (2015).
- Franklin, K. & Paxinos, G. *The Mouse Brain in Stereotaxic Coordinates* 3rd edn (Academic Press, 2008).

**Publisher's note** Springer Nature remains neutral with regard to jurisdictional claims in published maps and institutional affiliations.

© The Author(s), under exclusive licence to Springer Nature Limited 2021

## Methods

### Mice

All animal procedures followed the ethical guidelines outlined in the National Institutes of Health Guide for the Care and Use of Laboratory Animals, and all protocols were approved by the Institutional Animal Care and Use Committee (IACUC) at Harvard Medical School. Mice were maintained under constant temperature ( $23 \pm 1^\circ\text{C}$ ) and relative humidity ( $46 \pm 5\%$ ) with a 12-h light/dark cycle. Wild-type C57BL/6 (000664), *Agrp-ires-cre* (012899), *Isl-ChR2* (024109), *Isl-halorhodopsin* (014539), *Mc4r*-KO (006414), *Vgat-flox* (012897), *Npy*-KO (004545), *Npy1r*-KO (005408) and *Npy5r*-KO (007584) mice (>8 weeks old) were purchased from Jackson Laboratories.

### Two-choice odour preference test

Odour preference was measured using a previously described two-choice paradigm<sup>9</sup> with minor modifications. The test arena consisted of two odour applicators placed on each side of a plastic cage (M-BTM-STD, Innovive) without bedding. Odour applicators were Petri dishes (35 mm, Falcon, 351008) with 13 holes drilled in the lid to enable odours to escape. Test stimuli or water (400  $\mu\text{l}$ ) water were added just before testing, and the lid of the Petri dish was closed to prevent direct contact with the stimulus. Food odour was prepared by suspending 20 g of normal chow (LabDiet 5058, Lab Supply) in 50 ml water (4 h) and centrifuging (200g, 5 min) to remove insoluble material; mouse urine was freshly collected by hand. Mice were individually housed, naive to the paradigm, and tested in the dark phase. Fed and fasted mice were fasted for 24 h, and immediately before testing, fed mice were given free access to food for 1 h while fasted mice were not; mice fed ad libitum were never food restricted. Mate-exposed mice lived with a mate for 24 h immediately before isolation for fasting. Mice were habituated by successive administration ( $3 \times 5$  min) to mock test arenas containing blank odour applicators, and then introduced into the test arena. Odours were placed on each side of the arena in different tests, and no side bias was observed in control experiments involving water alone (Extended Data Fig. 1b). Mice were recorded with a digital video camera, and odour investigation scored manually, in a randomized double-blind manner, as time investigating each Petri dish over the entire test period (5 min). The position of the nose of the mouse was illustrated in Fig. 1 using Optimouse software<sup>32</sup>. Investigation time was quantified as the time in which the nose of the mouse was directly above an odour port, and preference index was calculated as the percentage of time spent investigating the food odour minus the percentage of time spent investigating pheromones. Rarely, data from mice were excluded if they did not investigate both odour sources during the two-choice odour test. Statistical analysis was performed using a Wilcoxon matched-pairs signed rank test. Sample sizes were based on previous publications involving two-choice odour tests<sup>9</sup>.

### Food intake measurement

Food intake was measured just before or after odour preference tests, as indicated in the timelines shown in the figures. Food and water were provided ad libitum in a clean cage, and the amount of food consumed over 1 h was measured by weighing food before and after the test period.

### Optogenetics

For surgical injection of AAV and implantation of optic fibres, mice were anaesthetized with avertin (250 mg kg<sup>-1</sup>) and placed into a stereotaxic device (KOPF). After exposing the skull via small incision, a small hole was drilled. For axonal activation of AGRP neurons, *AAV-DIO-ChR2* (Addgene 20297-AAV9, titre:  $3.1 \times 10^{13}$  genomes per ml) was injected bilaterally into the arcuate nucleus (bregma  $-1.45$  mm, midline  $\pm 0.20$  mm, skull surface  $-5.95$ ,  $-5.85$ ,  $-5.75$  mm, 50 nl per site) of *Agrp-ires-cre* mice using a pulled-glass pipette with a tip diameter of 20–40  $\mu\text{m}$ . A micromanipulator (Nanoject III, Drummond) was used to control

injection speed and volume, and the pipette was withdrawn 5 min after injection. Optic fibres (200  $\mu\text{m}$  core, NA 0.50, Thorlabs) with a ferrule (Thorlabs) were implanted unilaterally in either the arcuate nucleus (bregma  $-1.45$  mm, midline  $\pm 0$  mm, skull surface  $-5.6$  mm), BNST (bregma  $+0.62$  mm, midline  $+0.65$  mm, skull surface  $-4.40$  mm), PVH (bregma  $-0.94$  mm, midline  $\pm 0$  mm, skull surface  $-4.80$  mm), PVT (bregma  $-1.10$  mm, midline  $\pm 0$  mm, skull surface  $-3.20$  mm), CeA (bregma  $-1.10$  mm, midline  $+2.60$  mm, skull surface  $-4.35$  mm), LH (bregma  $-1.30$  mm, midline  $+1.00$  mm, skull surface  $-5.00$  mm), MeA (bregma  $-1.60$  mm, midline  $+2.00$  mm, skull surface  $-5.50$  mm), PAG (bregma  $-4.50$  mm, midline  $+0.50$  mm, skull surface  $-2.80$  mm) or PBN (bregma  $-5.20$  mm, midline  $+1.25$  mm, skull surface  $-3.20$  mm). Fibres were secured to the skull with dental cement and both fibres and ferrules were covered with caps (Thorlabs) for protection. Mice recovered from optic fibre surgery for 1 week, and from AAV injection with optic fibre surgery for 3 weeks. Optogenetic protocols were similar to previous reports<sup>15</sup>, and were initiated before the first habituation, and maintained for the duration of the odour-preference test and subsequent food intake test. Light was delivered (10-ms pulses, 20 pulses for 1 s, repeated every 4 s for activation or 1.5 s for inhibition, 6–8 mW to AGRP neuron soma and 6–10 mW to AGRP neuron axons) by LED (473 nm for activation, 625 nm for inhibition, Prizmatix) using a pulser (Prizmatix) through an optic fibre attached to the ferrule-capped optic fibre implanted in the mouse. Fibre placements were verified after each test by immunohistochemistry for AGRP (Neuromics GT15023, 1:100) and AAV injection sites were verified using AAV-derived mCherry fluorescence. Halorhodopsin function in AGRP neurons was validated by whole-cell current clamp recordings during optogenetic experiments (625 nm, 10-s continuous illumination, fibre output 6–8 mW) of acutely harvested and dissociated arcuate nucleus 2 h after attachment using a Molecular Device 700B amplifier with filtering at 1 kHz and 4–10 m $\Omega$  electrodes filled with an internal solution containing (in mM) 130 K-gluconate, 15 KCl, 4 NaCl, 0.5 CaCl<sub>2</sub>, 10 HEPES, 1 EGTA, pH 7.2, 290 mOsm, with cells bathed in an external solution containing (in mM) 150 NaCl, 2.8 KCl, 1 MgSO<sub>4</sub>, 1 CaCl<sub>2</sub>, 10 HEPES, pH 7.4, 300 mOsm.

### Food-odour learning paradigm

Before training, mice were food-restricted (2 g chow per day in a food bowl to maintain 85–95% body weight) for four days. For training (over the next four days), food-restricted mice were given strawberry sugar-free gelatin<sup>20</sup> (Conagra Brands, Snack Pack) ad libitum in a food bowl for 30 min once a day (during the dark period). After gelatin was removed, mice were left without food for 1 h, and then given 2.5 g chow per day (to maintain 80–90% body weight) to eat freely until the training period the next day. After the last day of training, mice were fasted as part of the two-choice odour test protocol instead of being given 2.5 g chow. During odour testing, strawberry gelatin (1 g) was placed in the odour applicator. In the pre-test trial when fasted (see Extended Data Fig. 4c), all mice were confirmed to prefer strawberry-gelatin odour after training. For optogenetics experiments, training occurred three weeks after placement of the optic fibre.

### Cell-specific NPY rescue

The plasmid to generate *AAV-DIO-Npy* was made by insertion of an *Npy-mCherry* gene (excised from Addgene 67156 with NheI and BsrGI) into an AAV vector (*pAAV-EF1a-DIO-hM3D(Gq)-mCherry*, Addgene 50460 cut with NheI and BsrGI, which removes *hM3D(Gq)-mCherry*). *AAV-DIO-Npy* was produced in HEK-293T cells with a particular capsid (*AAV-PHP.eB*, Addgene 103005) and AAV helper (Addgene 112867). *AAV-DIO-NPY* (titre  $10^{13}$  genomes per ml) was injected bilaterally into the arcuate nucleus (bregma  $-1.45$  mm, midline  $\pm 0.20$  mm, skull surface  $-5.95$ ,  $-5.85$ ,  $-5.75$  mm, 50 nl per site) of *Npy*-KO or *Agrp-ires-cre;Npy*-KO mice. Behavioural analysis was performed three weeks after AAV injection, and NPY expression was verified post hoc by immunohistochemistry for NPY (Peninsula Laboratories, 1:250, T-4070.0050).

## Administration of NPY5R ligands

An external cannula (26 gauge, Plastics One) and dummy internal cannula were implanted into the PVT (bregma  $-1.10$  mm, midline  $\pm 0$  mm, skull surface  $-2.20$  mm), dorsal third ventricle (bregma  $-1.10$  mm, midline  $\pm 0$  mm, skull surface  $-1.50$  mm) or ventral third ventricle (bregma  $-1.30$  mm, midline  $\pm 0$  mm, skull surface  $-4.70$  mm) and secured to the skull with dental cement. For injections, the dummy cannula was removed and an internal cannula (33 gauge, Plastics One) was inserted 1 mm beyond the external cannula for a final distance from the skull surface of  $-3.20$  mm (PVT),  $-2.50$  (dorsal third ventricle) or  $-5.70$  (ventral third ventricle). Test stimuli were injected by syringe ( $0.02 \mu\text{l min}^{-1}$ ) and included artificial cerebrospinal fluid (aCSF, TORCIS) alone, NPY ( $7.7 \mu\text{g} \mu\text{l}^{-1}$  in aCSF,  $0.02 \text{ mg kg}^{-1}$  except for ventral third ventricle injections in Extended Data Fig. 10, which involved  $0.2 \text{ mg kg}^{-1}$ , Bachem), NPY5R agonist ([CPP<sup>1-7</sup>, NPY<sup>19-23</sup>, Ala<sup>31</sup>, Aib<sup>32</sup>, Gln<sup>34</sup>]-hPancreatic Polypeptide,  $0.71 \mu\text{g} \mu\text{l}^{-1}$  in aCSF,  $0.002 \text{ mg kg}^{-1}$ , TOCRIS) and NPY5R antagonist (CGP71683 hydrochloride,  $51.7 \mu\text{g} \mu\text{l}^{-1}$  in aCSF,  $0.2 \text{ mg kg}^{-1}$ , TOCRIS). After injection (1 min later), the internal cannula was removed and the dummy cannula was re-inserted. Injections were performed immediately before habituation onset, except for the ventral third ventricle injections in Extended Data Fig. 10, which were performed 45 min before habituation onset. Cannula placements were verified by histology.

## Fibre photometry

For fibre photometry, *AgRP-ires-cre* mice were injected in the arcuate nucleus with AAV-DIO-GCaMP6s (Addgene, 100845-AAV9, titre  $2.1 \times 10^{13}$  genomes per ml), and a patch fibre (200 mm core diameter, 0.57 NA, metal ferrule, Doric) was inserted in the arcuate nucleus, PVT or PVH. Two weeks after surgery, fibre photometry was performed using an RZ10x real-time processor (Tucker-Davis Technologies). Light from connected 405 nm and 465 nm LEDs was filtered through a fluorescence minicube (Doric Lenses) and collected with an integrated photosensor on the RZ10x connected to the surgically implanted optic fibre with a 0.48 NA, 200  $\mu\text{m}$  core diameter patchcord (Doric Lenses). Fibre photometry was performed on fasted mice during a one-choice odour preference assay, which involved habituation ( $3 \times 5$  min), a water test (5 min), rest (2 min in habituation chamber), a pheromone test (5 min), rest (2 min in habituation chamber), and food-odour test (5 min). Ten minutes after the food-odour test, mice were given direct access to food in their home cage during fibre photometry. Changes in calcium-dependent GCaMP6s fluorescence (465 nm) signal were compared with calcium-independent GCaMP6s fluorescence (405 nm), providing an internal control for movement and photobleaching artefacts. Fluorescence measurements were made, extracted from Synapse software (Tucker-Davis Technology), and analysed in MATLAB (GraphPad). The fluorescence signal ( $F$ ) was defined as the ratio of fluorescence measured at 465 nm to the fluorescence measured at 405 nm;  $\Delta F/F$  value was expressed by comparing the fluorescence signal to a pre-test baseline, and a mean  $\Delta F/F$  was calculated for the time intervals indicated in the figures. Statistical analysis was performed using two-way ANOVA followed by a post hoc Bonferroni's multiple comparisons test; mice were excluded from analysis if AGRP neurons did not respond during food consumption after the odour test and/or if GCaMP expression or optic fibre placement was not properly targeted based on post hoc histology.

## Food search behaviour

Mice were fasted (24 h) or fed ad libitum, and briefly removed from their home cage to a fresh cage. While mice were absent from the home cage, a food pellet (3 g) was buried beneath bedding (depth  $> 1$  cm), and the mice were then re-introduced to the home cage. The latency to discover the food was recorded, and if the food was not discovered within 10 min, the trial was ended and the latency was recorded as 600 s.

## Single-colour RNA in situ hybridization

Coronal cryosections ( $16 \mu\text{m}$ ) of freshly frozen mouse brain were washed with PBS, treated with proteinase K (Thermo Fisher Scientific,  $10 \text{ mg ml}^{-1}$ ,

$10 \text{ mM}$  Tris-Cl (pH 7.4) with  $1 \text{ mM}$  EDTA (pH 8.0), 10 min,  $37^\circ\text{C}$ ), fixed (4% PFA, PBS, 10 min), washed (PBS, 5 min), acetylated (0.25% acetic anhydride, 1.3% triethanolamine, 0.25% HCl, in water, 10 min), washed (PBS, 5 min), dried and pre-hybridized ( $60^\circ\text{C}$ , 1 h) in hybridization buffer (50% formamide, 0.6 M NaCl, 10 mM Tris-Cl (pH 8.0), 5 mM EDTA, 0.3  $\text{mg ml}^{-1}$  yeast-tRNA, 1x Denhalt's solution, 0.1  $\text{mg ml}^{-1}$  heparin, 0.1% Tween-20, 0.25% SDS, in DEPC-treated water). Digoxigenin-labelled cRNA probes were transcribed using T3 RNA polymerase from PCR-derived DNA templates amplified using the following primer pairs: *Npy5r-antisense* (899 bp) TGCCATTCCTTCAGTGTGTATC and AATTAACCCTCACTAAAGGGGACATCATGCCTAACAAAGTGA; *Npy5r* sense (899 bp): AATTAACCCTCACTAAAGGGTGCCTTCAGTGTGTATC and GGACATCATGCCTAACAAAGTGA; treated with DNase I (Roche Applied Science, 20 min,  $37^\circ\text{C}$ ) and purified (ProbeQuant G-50 Columns, GE Healthcare). RNA probe ( $1.5 \text{ ng} \mu\text{l}^{-1}$  in hybridization buffer) was preheated ( $85^\circ\text{C}$ , 5 min), cooled on ice and applied to each slide (200  $\mu\text{l}$  beneath Parafilm in a chamber equilibrated with 50% formamide, 16 h,  $60^\circ\text{C}$ ). Sections were washed (1:  $5 \times$  SSC (3 min,  $65^\circ\text{C}$ ); 2:  $2 \times$  SSC/50% formamide (20 min,  $65^\circ\text{C}$ ); 3:  $0.2 \times$  SSC ( $2 \times 20$  min,  $65^\circ\text{C}$ )), blocked (1 h, room temperature) in blocking buffer (1% blocking reagent (Roche Applied Science, 11096176001), 100 mM maleic acid, pH 8.0, 150 mM NaCl, 0.3% Tween-20), and incubated with primary antibody (horseradish peroxidase conjugated anti-digoxigenin antibody (Roche Applied Science 11207733910), 1:500 in blocking buffer, overnight,  $4^\circ\text{C}$ ). The next day, slides were washed ( $3 \times 10$  min, PBST), treated with TSA Plus Cyanine 3 (PerkinElmer, NEL744001KT, 1:70 in  $1 \times$  plus amplification diluent, 20 min), washed ( $1 \times 10$  min, PBST) mounted with cover glass using Fluoromount with 4',6-diamidino-2-phenylindole dihydrochloride (Southern BioTech 0100-20), and analysed by fluorescence microscopy.

## Reporting summary

Further information on research design is available in the Nature Research Reporting Summary linked to this paper.

## Data availability

All raw data points used for statistical analysis (Prism software) and to generate graphs are reported directly in the figures. Exact  $P$  values for pairwise data comparisons in figures, from left to right, using the tests described in the figure legends, are as follows: Fig. 1b: 0.85, 0.002; Fig. 1d: 0.77, 0.002; Fig. 2b (control): 0.82, 0.69, 0.44, 0.56, 0.69, 0.69, 0.69, 0.56, 0.77; Fig. 2b (AGRP-ON): 0.38, 0.69, 0.008, 0.57,  $>0.99$ , 0.16, 0.69, 0.31, 0.002; Fig. 2c:  $<0.0001$ , 0.0003, 0.0007, 0.0004, 0.29, 0.89, 0.34, 0.59,  $<0.0001$ ; Fig. 2d: 0.03, 0.84; Fig. 3b (fed): 0.23, 0.38, 0.56; Fig. 3b (fasted): 0.002, 0.002, 0.63; Fig. 3d: 0.30, 0.0005; Fig. 3e: 0.002; 0.85; Fig. 3h:  $>0.99$ , 0.03, 0.03; Fig. 3i: 0.03, 0.84. Source data are provided with this paper.

32. Ben-Shaul, Y. OptiMouse: a comprehensive open source program for reliable detection and analysis of mouse body and nose positions. *BMC Biol.* **15**, 41 (2017).

**Acknowledgements** We thank B. Lowell, M. Andermann, S. Datta, M. Albers, J. Flanagan, C. Ran and K. Tao for comments on the manuscript; Q. Li and K. Tao for experimental assistance; and the Nikon Imaging Center at Harvard Medical School for microscopy assistance. The work was supported by a National Institutes of Health grant to S.D.L. (R01 DC013289) and a Uehara Memorial Foundation postdoctoral fellowship and Mishima Kaiun Memorial Foundation funding to N.H. S.D.L. is an investigator of the Howard Hughes Medical Institute.

**Author contributions** N.H. and S.D.L. designed the experiments, N.H. performed the experiments and S.D.L. wrote the manuscript.

**Competing interests** The authors declare no competing interests.

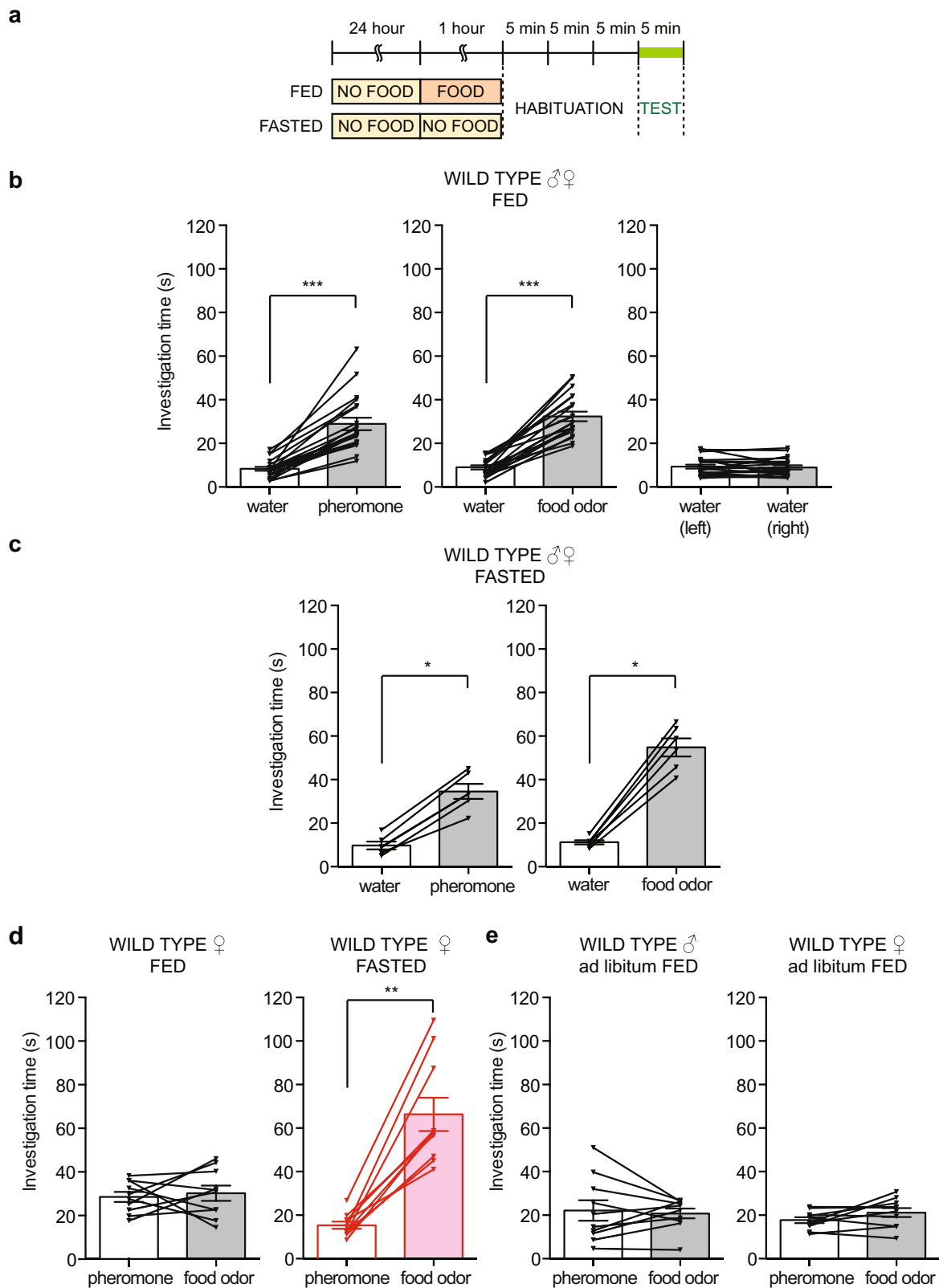
## Additional information

**Supplementary information** The online version contains supplementary material available at <https://doi.org/10.1038/s41586-021-03299-4>.

**Correspondence and requests for materials** should be addressed to S.D.L.

**Peer review information** Nature thanks Michael Krashes and the other, anonymous, reviewer(s) for their contribution to the peer review of this work.

**Reprints and permissions information** is available at <http://www.nature.com/reprints>.

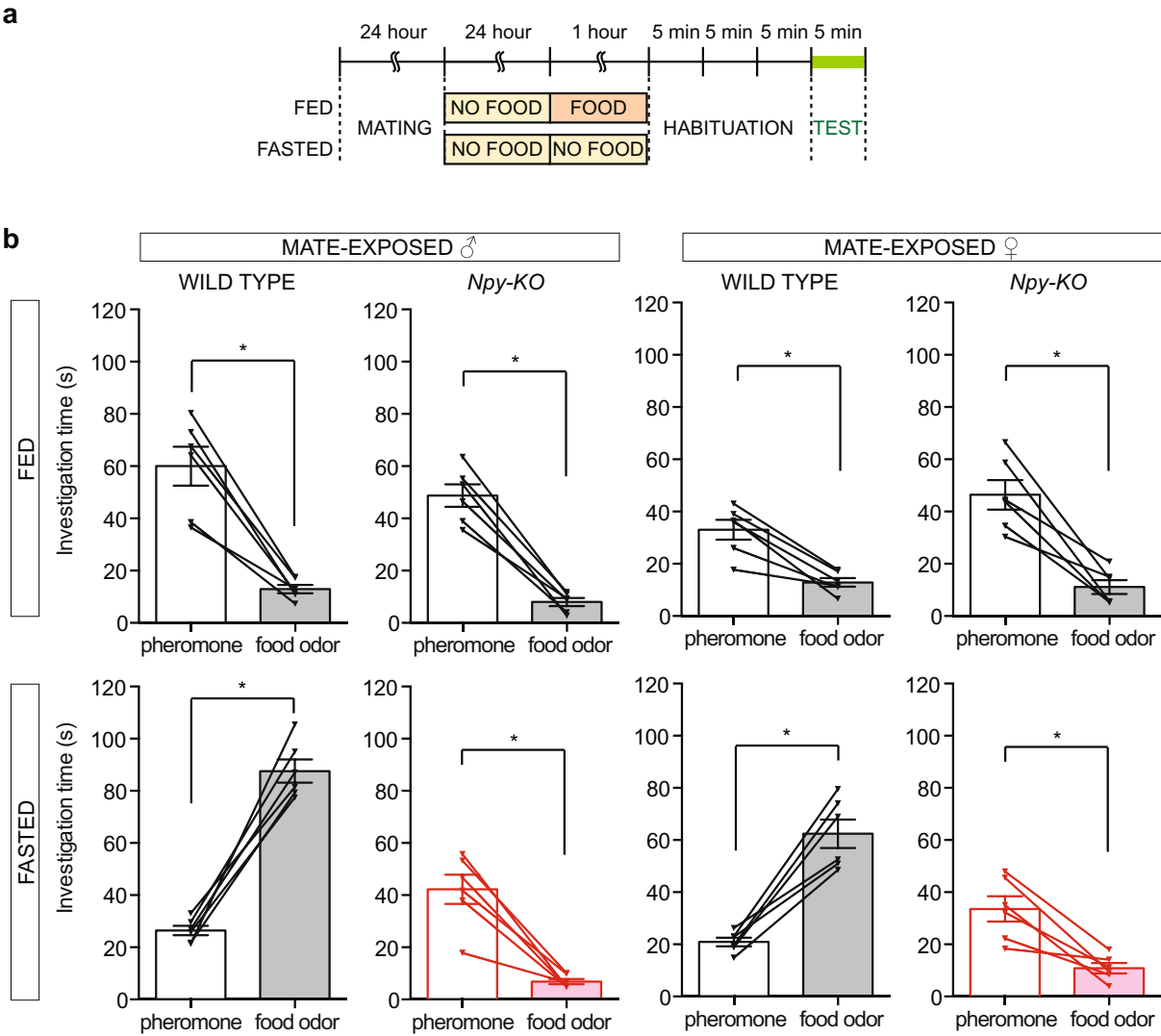


**Extended Data Fig. 1 | Controls for two-choice odour-preference assay.**

**a**, Timeline of two-choice behavioural assay. **b, c**, Odour investigation times of fed (**b**) and fasted (**c**) male and female wild-type mice in single odour pairings with water. *n* (for **b**) = 10 male mice and 10 female mice; *n* (for **c**) = 3 male and 3 female mice. Data are mean  $\pm$  s.e.m., lines with triangles represent individual mice. \* $P$  < 0.05, \*\*\* $P$  < 0.001, two-tailed Wilcoxon test (*P* left to right in **b**: < 0.0001, < 0.0001, 0.86; *P* left to right in **c**: 0.03, 0.03). A statistical comparison of odour responses in **b** and **c** using a two-tailed Mann-Whitney *U*-test revealed

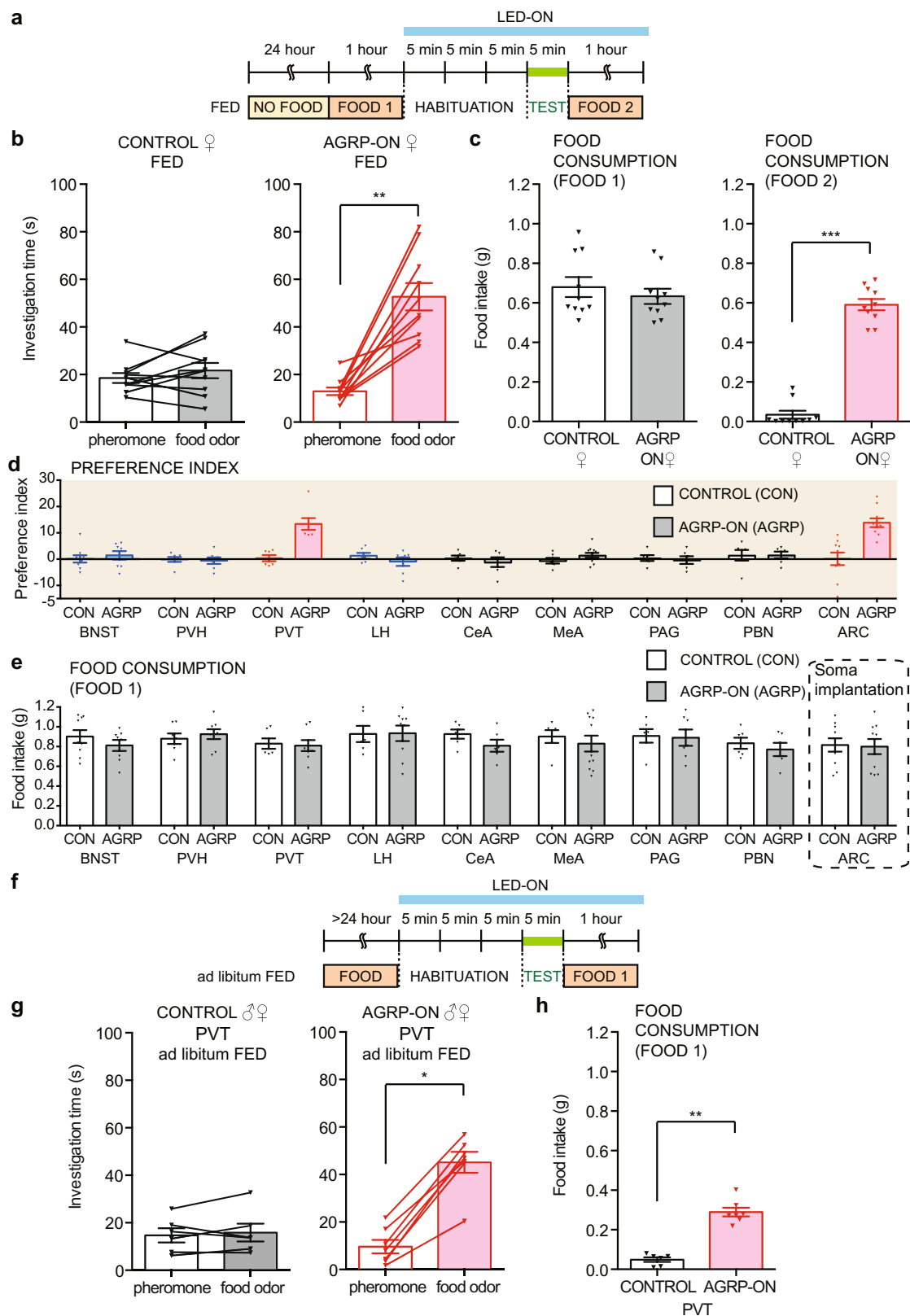
significant increases in food-odour investigation in fasted mice compared with fed mice ( $P$  = 0.0006) but not in pheromone investigation ( $P$  = 0.15). **d**, Odour investigation times of fed (left) and fasted (right) wild-type female mice. *n* = 10 mice, data are mean  $\pm$  s.e.m., lines with triangles represent individual mice. \*\* $P$  < 0.01, two-tailed Wilcoxon test (*P* fed: 0.77, *P* fasted: 0.002). **e**, Odour-investigation times of male (left) and female (right) wild-type mice fed ad libitum. *n* = 10 mice, data are mean  $\pm$  s.e.m., lines with triangles represent individual mice, *P* male, 0.92; *P* female, 0.19; two-tailed Wilcoxon test.





**Extended Data Fig. 2 | Mate encounters selectively enhance pheromone attraction in fed mice through an NPY-independent mechanism.**  
**a, b,** Timeline of two-choice behavioural assay (**a**) and odour-investigation times (**b**) after mate exposure, fed (top) and fasted (bottom), male (left) and

female (right), wild-type and *Npy*-KO mice.  $n = 6$  mice, data are mean  $\pm$  s.e.m., lines with triangles represent individual mice. \* $P < 0.05$ , two-tailed Wilcoxon test.  $P$  left to right, fed: 0.03, 0.03, 0.03, 0.03;  $P$  left to right, fasted: 0.03, 0.03, 0.03, 0.03.

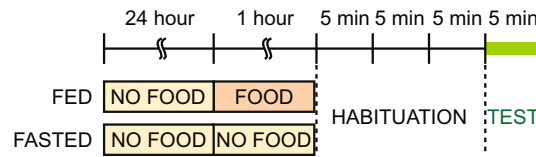


**Extended Data Fig. 3** | See next page for caption.

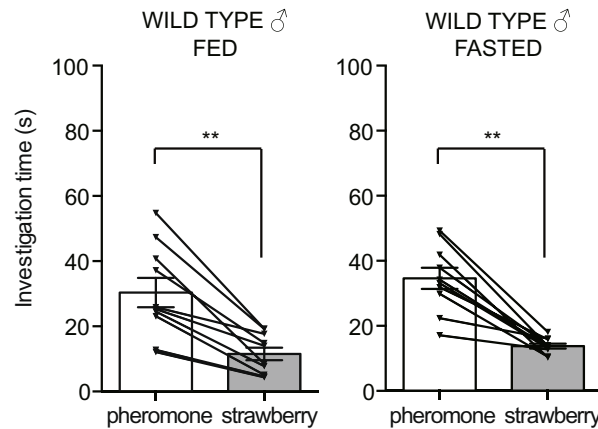
**Extended Data Fig. 3 | Controls for experiments involving optogenetic stimulation of AGRP neuron projections to the PVT.** **a**, Timeline of two-choice assay involving optogenetic stimulation (blue bar) of AGRP neurons. **b**, Investigation times of fed control (black) and fed AGRP-ON (red) female mice to pheromones and food odours.  $n = 10$  mice, data are mean  $\pm$  s.e.m., lines with triangles represent individual mice.  $**P < 0.01$ , two-tailed Wilcoxon test ( $P$  control: 0.32;  $P$  AGRP-ON: 0.02). **c**, Food intake was measured before (Food 1) and after (Food 2) the odour preference assay, as indicated in the timeline, for female mice used in **b**.  $n = 10$  mice, data are mean  $\pm$  s.e.m., triangles represent individual mice,  $***P < 0.001$ , Mann-Whitney  $U$ -test ( $P$  Food 1: 0.49;  $P$  Food 2:  $< 0.0001$ ). **d**, Preference indices were calculated for fed control (unfilled bars, CON) and fed AGRP-ON (filled bars, AGRP) mice after illumination of brain regions indicated ( $n$  values are as reported for the same mice in Fig. 2b, c, data are mean  $\pm$  s.e.m.). **e**, Food intake before two-choice assay and optogenetic

stimulation (Food 1 in timeline) of mice with optic fibres implanted in various brain regions ( $n$  values are as reported for the same mice in Fig. 2b, c, data are mean  $\pm$  s.e.m.,  $P$  values by Mann-Whitney  $U$ -test from left to right: 0.47, 0.52, 0.90, 0.94, 0.18, 0.95, 0.81, 0.57, 0.89). **f**, Timeline of two-choice behavioural assay involving optogenetic stimulation (blue bar) of AGRP neurons in mice fed ad libitum. **g**, **h**, *AAV-DIO-ChR2* was injected in the arcuate nucleus of wild-type (control) or *AgRP-ires-cre* (AGRP-ON) mice, and optic fibres were inserted in the PVT. Odour investigation times in the two-choice behavioural assay (**g**) and post-test food consumption (**h**, Food 1 from timeline in **f**) from indicated mice fed ad libitum.  $n = 6$  (control) and 7 (AGRP-ON) mice, data are mean  $\pm$  s.e.m., lines with triangles represent individual mice.  $*P < 0.05$ ,  $**P < 0.01$  ( $P$  values by two-tailed Wilcoxon test in **g**: 0.56, 0.02;  $P$  value by two-tailed Mann-Whitney  $U$ -test in **h**: 0.0012).

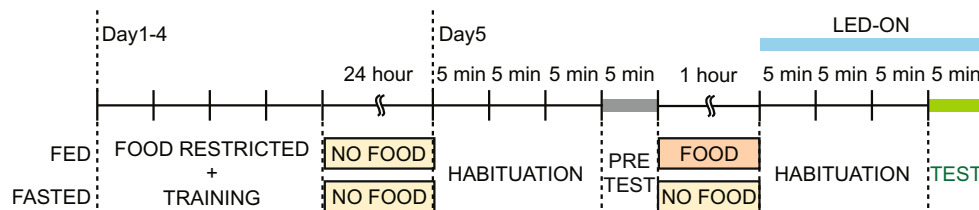
**a** BEFORE TRAINING



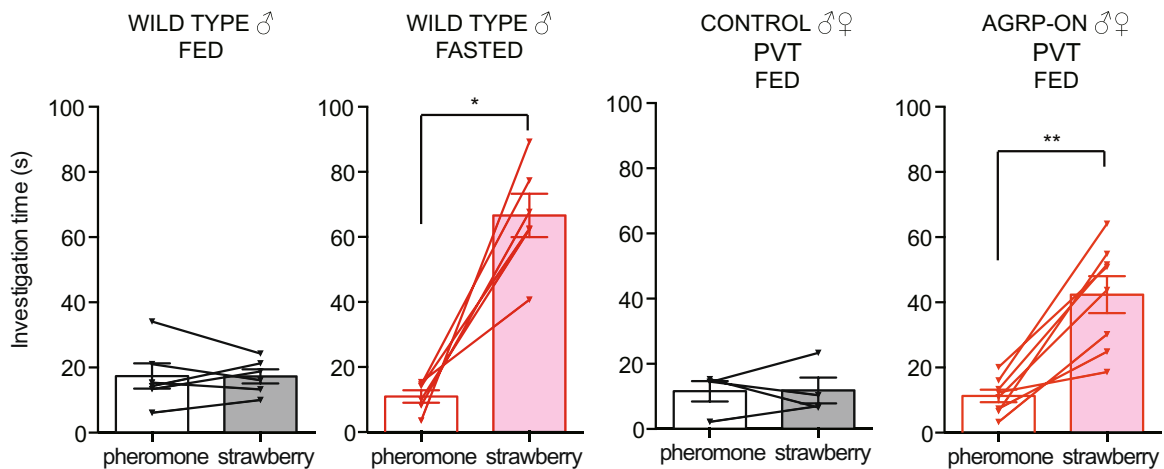
**b**



**c** AFTER TRAINING



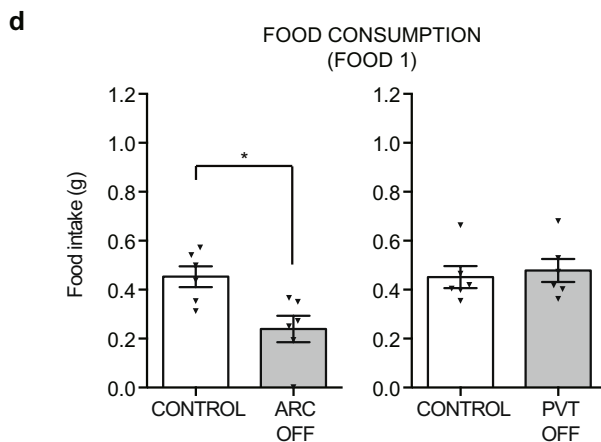
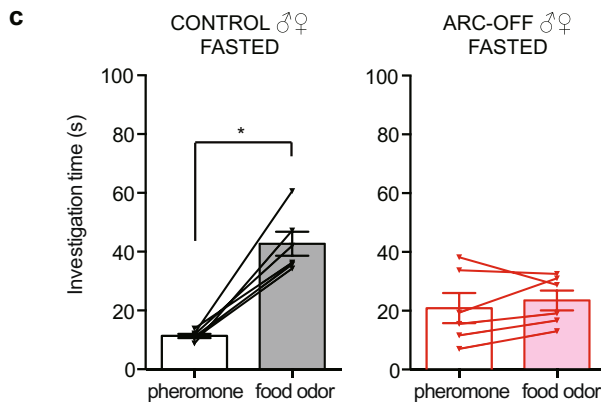
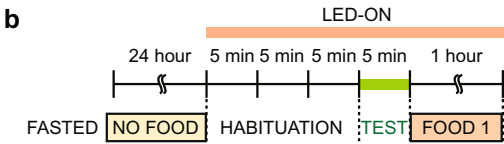
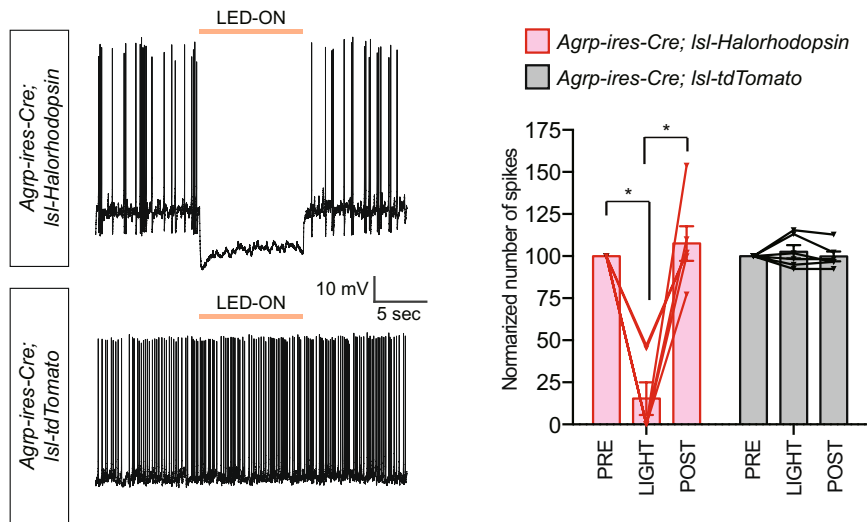
**d**



**Extended Data Fig. 4 | Attraction to a newly learned food odour is enhanced by hunger and optogenetic stimulation.** **a**, Timeline of two-choice behavioural assay before learning. **b**, Investigation times of fed (left) and fasted (right) wild-type male mice to pheromones (unfilled bars) and strawberry-gelatin odour (filled bars) before learning.  $n = 10$  mice, data are mean  $\pm$  s.e.m., lines with triangles represent individual mice.  $**P < 0.01$ , two-tailed Wilcoxon test ( $P_{\text{fed}}: 0.002$ ;  $P_{\text{fasted}}: 0.002$ ). **c**, Timeline of learning paradigm and two-choice behavioural assay after learning. **d**, Investigation

times to pheromones (unfilled bars) and strawberry-gelatin odour (filled bars) after learning in wild-type fed mice, wild-type fasted mice, wild-type fed mice after arcuate nucleus injection of *AAV-DIO-ChR2* and PVT illumination (control), and *AgRP-ires-cre* fed mice after arcuate nucleus injection of *AAV-DIO-ChR2* and PVT illumination.  $n = 6$  (wild-type fed, fasted), 4 (control, PVT) and 8 (AGRP-ON, PVT) mice, data are mean  $\pm$  s.e.m., lines with triangles represent individual mice.  $*P < 0.05$ ,  $**P < 0.01$ , two-tailed Wilcoxon test ( $P$  values from left to right:  $>0.99$ , 0.03, 0.88, 0.008).

**a** AGRP NEURON, CURRENT CLAMP ELECTROPHYSIOLOGY

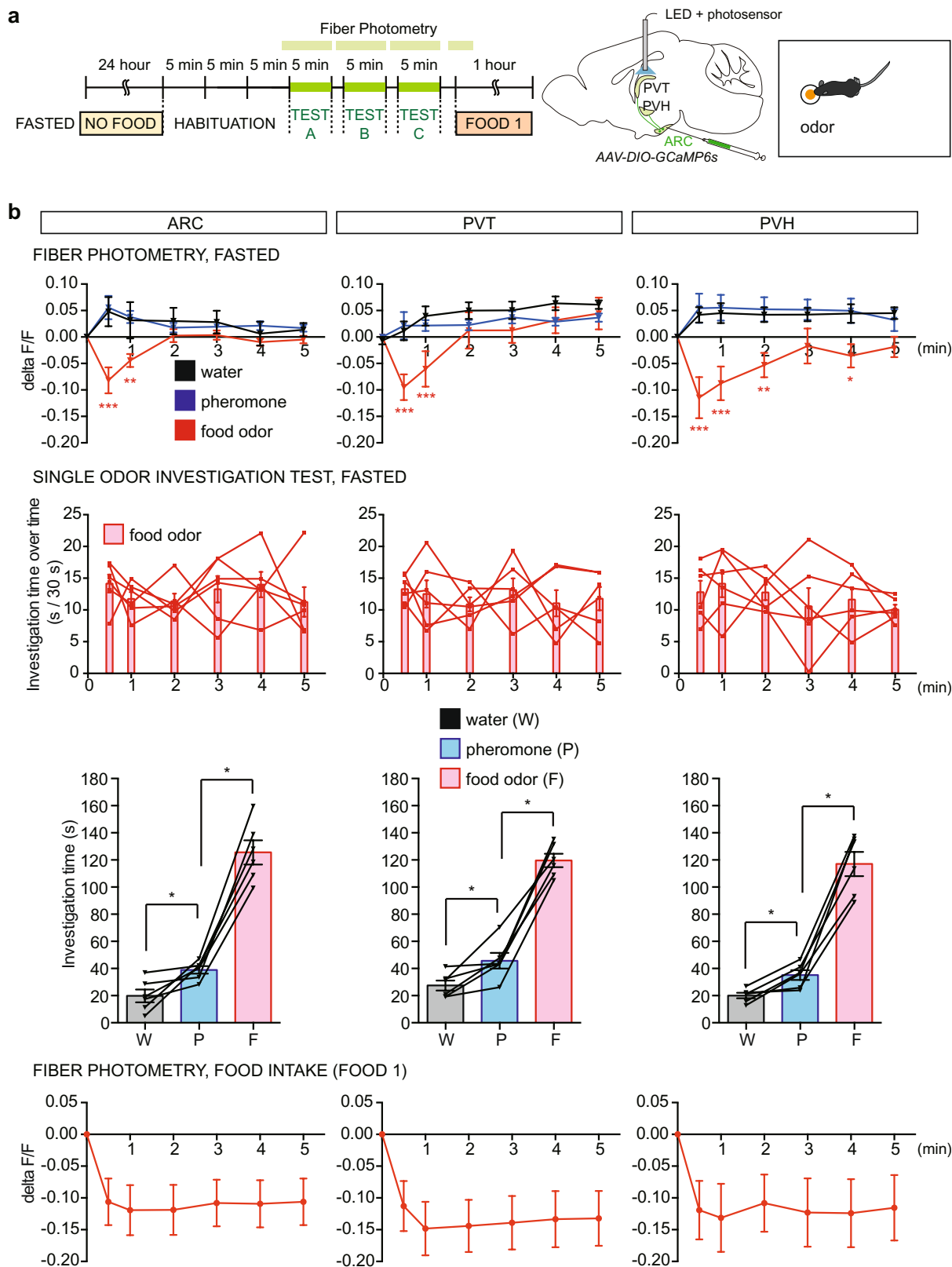


**Extended Data Fig. 5 | Controls for optogenetic inhibition experiments.**

**a**, AGRP neurons from *AgRP-ires-cre; Isl-halorhodopsin* (halorhodopsin is expressed as a fusion protein with YFP) or *AgRP-ires-cre; Isl-tdTomato* mice were dissociated and responses to light (LED-ON) were measured by whole-cell current clamp recordings. Representative examples (left) and the number of spikes measured (right) across cells from different mice before, during and after photostimulation with normalization to the pre-illumination period.  $n = 6$  cells, data are mean  $\pm$  s.e.m., lines represent individual cells. \* $P < 0.05$  by two-tailed Wilcoxon test ( $P$  pink pre versus light: 0.03,  $P$  pink light versus post: 0.03,  $P$  grey pre versus light: 0.78,  $P$  grey light versus post: 0.38). An additional statistical test involving one-way ANOVA with Tukey's multiple comparisons test revealed similar results (pink one-way ANOVA:  $P = 0.0003$ , with Tukey's multiple comparisons test: pre versus light:  $P < 0.0001$ , light versus post:  $P < 0.001$ , grey one-way ANOVA:  $P = 0.53$ ).

**b**, Timeline and schematic based on published brain section images<sup>31</sup> of optogenetic inhibition experiments in PVT. **c**, Investigation times in the two-choice behavioural assay during arcuate nucleus illumination in *AgRP-ires-cre* (control) or *AgRP-ires-cre; Isl-halorhodopsin* (ARC-OFF) mice.  $n = 6$  mice, data are mean  $\pm$  s.e.m., lines with triangles represent individual mice, \* $P < 0.05$  by two-tailed Wilcoxon test ( $P$  control: 0.03;  $P$  ARC-OFF: 0.44). **d**, Food consumption after the two-choice odour test (Food 1 in timeline) in *AgRP-ires-cre* (control) or *AgRP-ires-cre; Isl-halorhodopsin* (ARC-OFF, PVT-OFF) mice during ARC (left) or PVT (right) illumination.  $n = 6$  mice, mean  $\pm$  s.e.m., lines with triangles represent individual mice. \* $P < 0.05$ , two-tailed Mann-Whitney  $U$ -test ( $P$  left: 0.015,  $P$  right: 0.57).



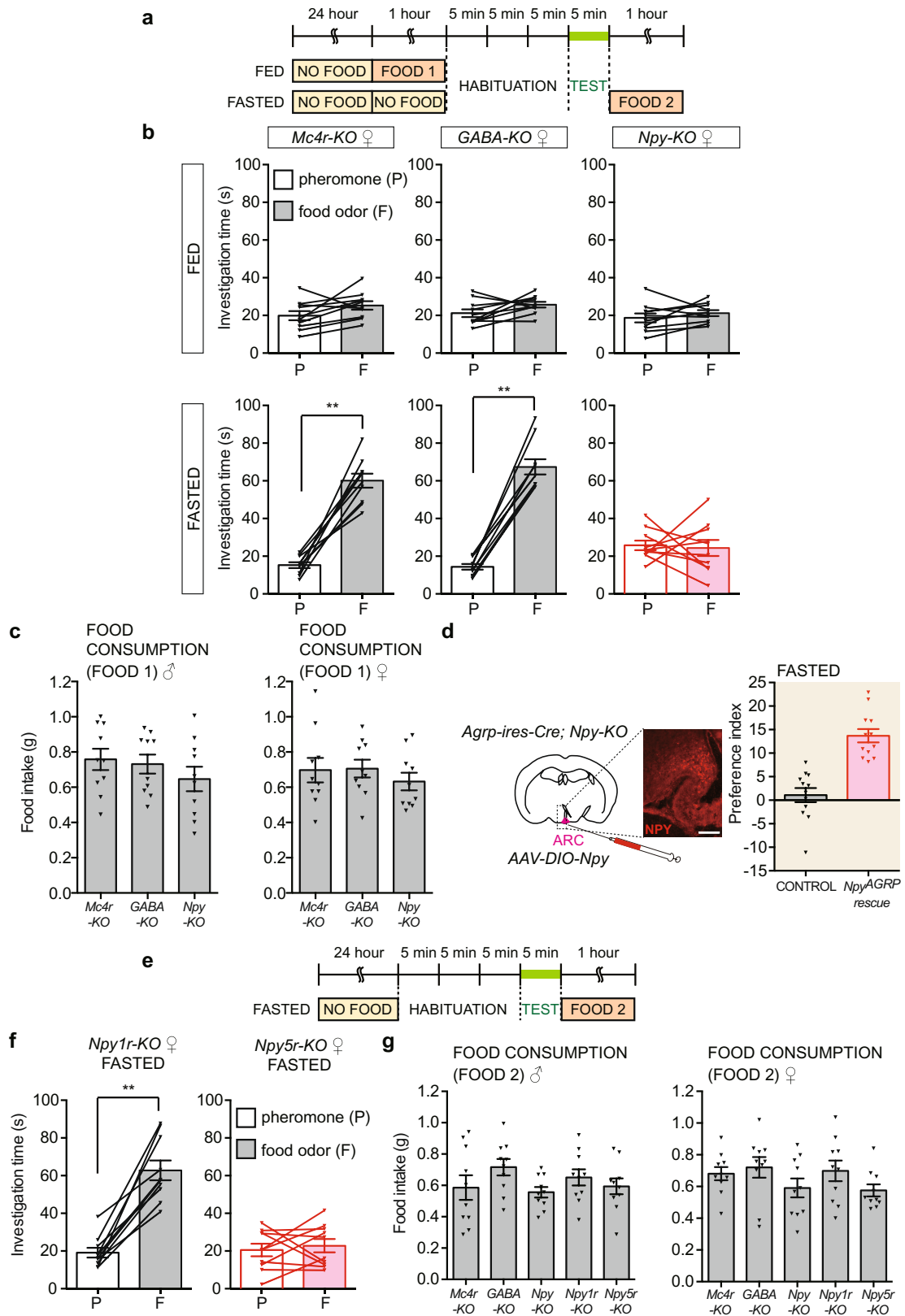


**Extended Data Fig. 6** | See next page for caption.

## Extended Data Fig. 6 | Food-odour investigation persists beyond transient decreases in AGRP neuron activity, as measured by fibre photometry.

**a**, Timeline and depiction of fibre photometry experiments during single-odour investigation, with schematic based on published brain section images<sup>31</sup>. *Agrp-ires-cre* mice were injected in the arcuate nucleus (ARC) with *AAV-DIO-GCaMP6s*, and fibre photometry was performed in the ARC, PVT or PVH during water investigation (Test A), pheromone investigation (Test B), food-odour investigation (Test C), and food consumption (Food 1). **b**, Top row, changes in GCaMP6s fluorescence ( $\Delta F/F$ ) were recorded by fibre photometry in brain regions indicated during single-odour investigation. Responses are depicted as the mean of measurements made in indicated time intervals (0–30 s, 30–60 s or each subsequent minute).  $n = 6$  mice, mean  $\pm$  s.e.m.,

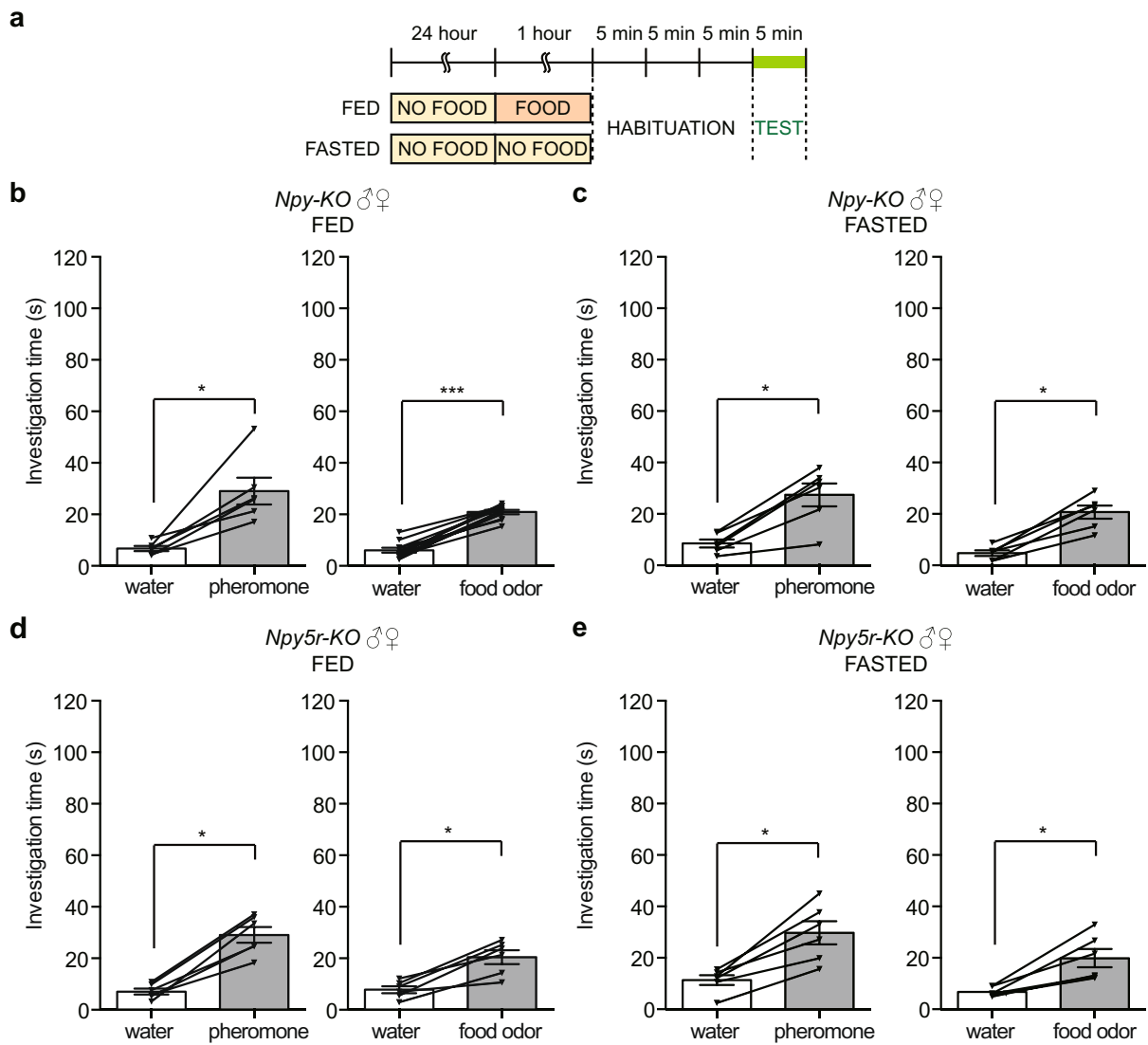
$*P < 0.05$ ,  $**P < 0.01$ ,  $***P < 0.001$ , statistical comparisons between food odour and water responses by two-way ANOVA with Dunnett's multiple comparison. Second row, food-odour investigation times per 30 s during fibre photometry measurements above at various time intervals (0–30 s, 30–60 s or each subsequent minute).  $n = 6$  mice, data are mean  $\pm$  s.e.m., lines represent individual mice. Third row, total investigation times for food odour, pheromones and water during 5-min fibre photometry test.  $n = 6$  mice, data are mean  $\pm$  s.e.m., lines with triangles represent individual mice,  $*P < 0.05$  by two-tailed Wilcoxon test ( $P$  water versus pheromone: 0.03;  $P$  pheromone versus food odour: 0.03 for ARC, PVT, PVH). Bottom row, changes in GCaMP6s fluorescence ( $\Delta F/F$ ) were recorded by fibre photometry during food consumption (Food 1 in timeline of **a**) after odour tests in the same mice.



**Extended Data Fig. 7** | See next page for caption.

**Extended Data Fig. 7 | Odour preferences and food consumption patterns in knockout and rescue mice.** **a**, Timeline of two-choice behavioural assay. **b**, Investigation times for pheromones and food odours in fed (top) and fasted (bottom) in the indicated female mice.  $n = 10$  mice, data are mean  $\pm$  s.e.m., lines with triangles represent individual mice.  $**P < 0.01$ , two-tailed Wilcoxon test (from left to right,  $P$  fed: 0.08, 0.16, 0.24;  $P$  fasted: 0.002, 0.002, 0.85). **c**, Food intake before two-choice assay (Food 1 in timeline) of various knockout male (left) and female (right) mice.  $n = 10$  mice, data are mean  $\pm$  s.e.m., triangles represent individual mice. **d**, Cartoon (left) and preference indices (right) of NPY rescue experiments involving *Npy*-KO (control) and *Agrp-ires-cre;Npy*-KO (*Npy*<sup>AGRP</sup> rescue) mice three weeks after *AAV-lsl-Npy* injection in the arcuate

nucleus. The schematic of the brain is based on published brain section images<sup>31</sup>. NPY immunohistochemistry is depicted in the figure inset. Preference indices are derived from data in Fig. 3d ( $n = 12$  mice, males and females, mean  $\pm$  s.e.m. Scale bar, 100  $\mu$ m). **e**, Timeline of two-choice behavioural assay for receptor knockouts. **f**, Investigation times for pheromones and food odours in the fasted female mice indicated.  $n = 10$  mice, data are mean  $\pm$  s.e.m., lines with triangles represent individual mice.  $**P < 0.01$ , two-tailed Wilcoxon test. (*PNpy1r*-KO: 0.02; *PNpy5r*-KO: 0.77). **g**, Food intake after two-choice assay (Food 2 in timeline) of the indicated male and female mice.  $n = 10$  mice, data are mean  $\pm$  s.e.m., triangles represent individual mice.

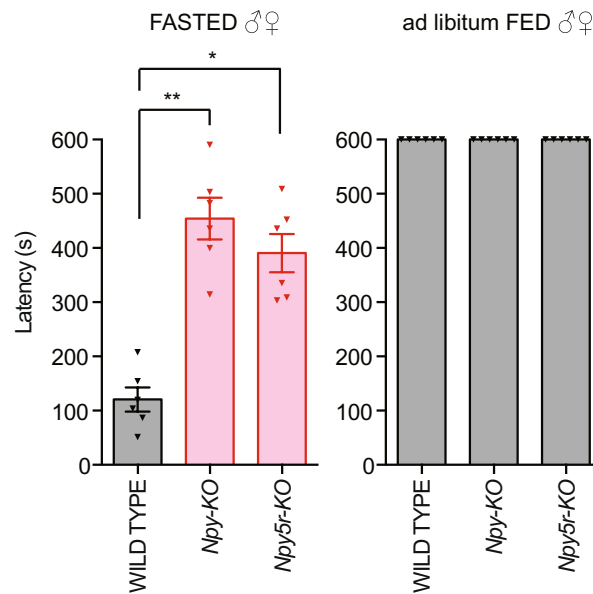
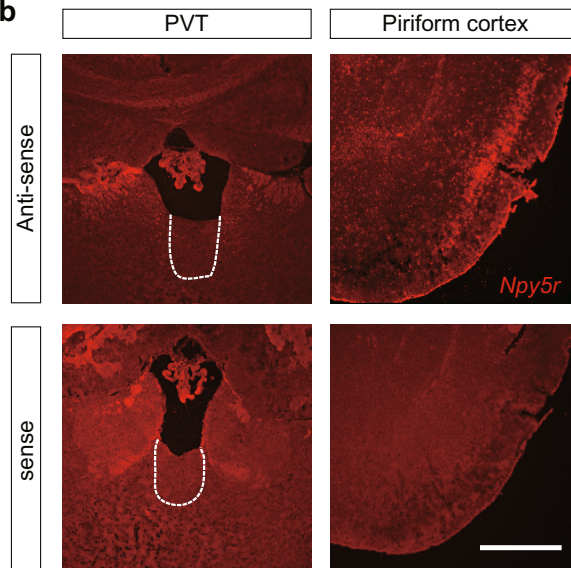
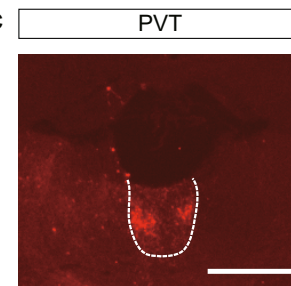


**Extended Data Fig. 8 | Single-odour preference assays in knockout mice.**

**a**, Timeline of behavioural assay. **b–e**, Odour investigation times of fed *Npy*-KO (**b**), fasted *Npy*-KO (**c**), fed *Npy5r*-KO (**d**) and fasted *Npy5r*-KO (**e**) mice in single-odour pairings with water.  $n = 3$  male mice and 3 female mice,

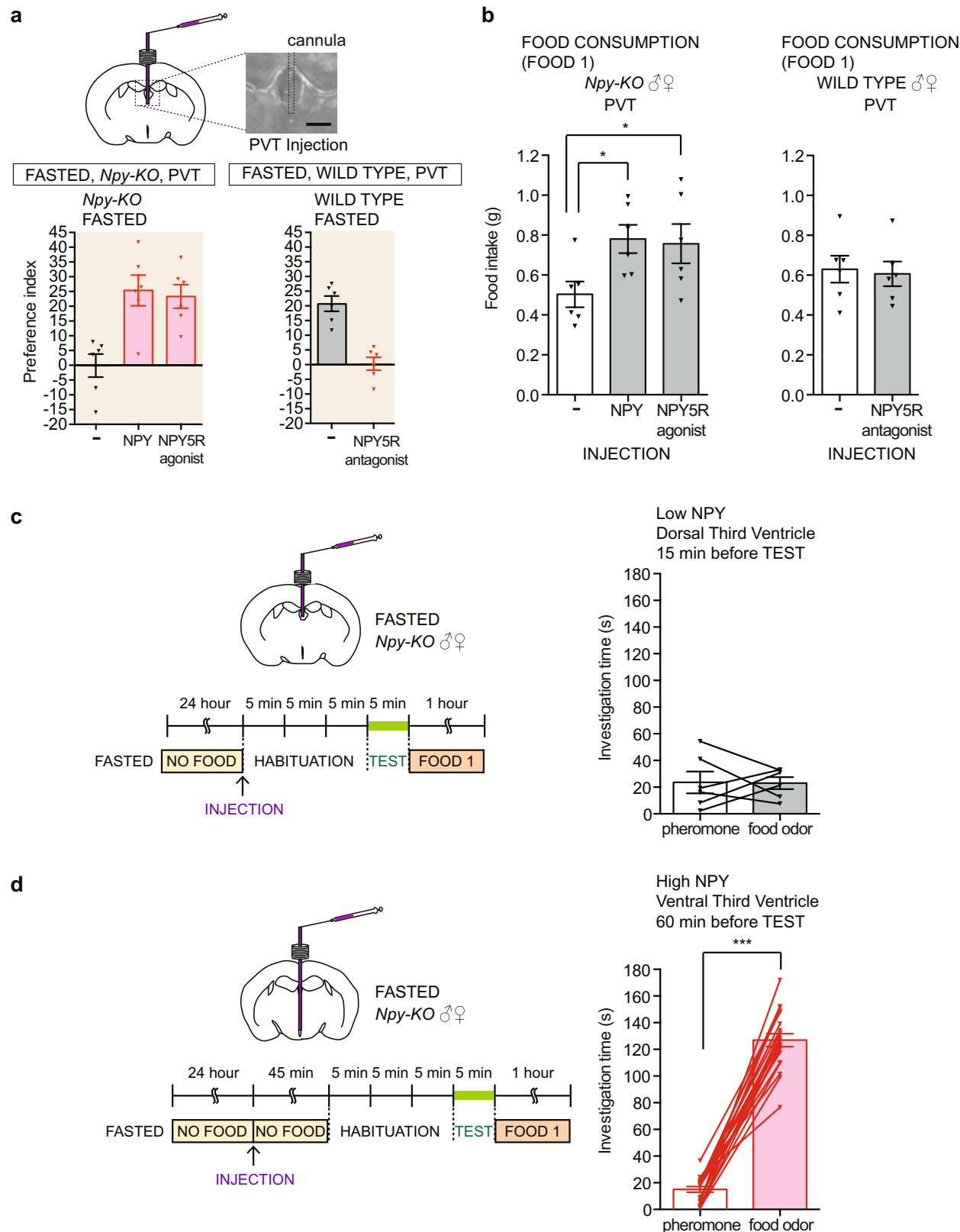
data are mean  $\pm$  s.e.m., lines with triangles represent individual mice. \* $P < 0.05$ , \*\* $P < 0.01$ , two-tailed Wilcoxon test ( $P$  values for **b**: 0.03, 0.001; **c**: 0.03, 0.03; **d**: 0.03, 0.03; **e**: 0.03, 0.03).



**a** FOOD SEARCH BEHAVIOR**b****c**

**Extended Data Fig. 9 | Food-search behaviour in knockout mice and analysis of *Npy5r* expression.** **a**, Latency to discover a food pellet buried in bedding was timed in the indicated fasted (left) and fed (right) mice.  $n = 3$  male mice and 3 female mice, data are mean  $\pm$  s.e.m. \*\* $P < 0.01$ , \* $P < 0.05$ , Kruskal-Wallis test with Dunn's multiple comparison. **b**, RNA in situ hybridization using *Npy5r* anti-sense and sense probes in coronal brain cryosections with PVT

(left, dashed lines) and piriform cortex. Scale bar, 500  $\mu$ m. **c**, AGRP neuron projections to the PVT were visualized by immunohistochemistry for tdTomato in *Agrp-ires-dre* mice injected in the arcuate nucleus with *AAV-DIO-tdTomato*. Scale bar, 500  $\mu$ m. Images in **b** and **c** are representative of three independent experiments involving different mice.



**Extended Data Fig. 10 | Controls for NPY injection into PVT.** **a**, Schematic depicting injection site (top) and preference indices for experiments in Fig. 3h, i.  $n = 10$  male mice and 10 female mice, data are mean  $\pm$  s.e.m. **b**, Post-test food consumption (Food 1) for mice in Fig. 3h, i.  $n = 3$  male mice and 3 female mice, data are mean  $\pm$  s.e.m., triangles represent individual mice. \* $P < 0.05$ , two-tailed Mann-Whitney  $U$ -test ( $P$ NPY versus control: 0.015;  $P$ NPY5R agonist versus control, 0.04). **c**, Fasted *Npy*-KO mice were injected with low NPY levels ( $0.02 \text{ mg kg}^{-1}$ ) in the dorsal third ventricle, and after 15 min behaviour was

analysed in the two-choice odour preference assay.  $n = 6$  (3 male mice and 3 female mice), data are mean  $\pm$  s.e.m., lines with triangles represent individual mice.  $P > 0.99$ , two-tailed Wilcoxon test. **d**, Fasted *Npy*-KO mice were injected with high NPY levels ( $0.2 \text{ mg kg}^{-1}$ ) in the ventral third ventricle, and after 60 min behaviour was analysed in the two-choice odour preference assay.  $n = 20$  (10 male mice and 10 female mice), data are mean  $\pm$  s.e.m., lines with triangles represent individual mice. \*\*\* $P < 0.001$ , two-tailed Wilcoxon test. Brain schematics are based on published brain section images<sup>31</sup>.

## Reporting Summary

Nature Research wishes to improve the reproducibility of the work that we publish. This form provides structure for consistency and transparency in reporting. For further information on Nature Research policies, see [Authors & Referees](#) and the [Editorial Policy Checklist](#).

### Statistics

For all statistical analyses, confirm that the following items are present in the figure legend, table legend, main text, or Methods section.

n/a Confirmed

- ☐ ☒ The exact sample size ( $n$ ) for each experimental group/condition, given as a discrete number and unit of measurement
- ☐ ☒ A statement on whether measurements were taken from distinct samples or whether the same sample was measured repeatedly
- ☐ ☒ The statistical test(s) used AND whether they are one- or two-sided  
*Only common tests should be described solely by name; describe more complex techniques in the Methods section.*
- ☐ ☒ A description of all covariates tested
- ☐ ☒ A description of any assumptions or corrections, such as tests of normality and adjustment for multiple comparisons
- ☐ ☒ A full description of the statistical parameters including central tendency (e.g. means) or other basic estimates (e.g. regression coefficient) AND variation (e.g. standard deviation) or associated estimates of uncertainty (e.g. confidence intervals)
- ☐ ☒ For null hypothesis testing, the test statistic (e.g.  $F$ ,  $t$ ,  $r$ ) with confidence intervals, effect sizes, degrees of freedom and  $P$  value noted  
*Give  $P$  values as exact values whenever suitable.*
- ☒ ☐ For Bayesian analysis, information on the choice of priors and Markov chain Monte Carlo settings
- ☒ ☐ For hierarchical and complex designs, identification of the appropriate level for tests and full reporting of outcomes
- ☒ ☐ Estimates of effect sizes (e.g. Cohen's  $d$ , Pearson's  $r$ ), indicating how they were calculated

*Our web collection on [statistics for biologists](#) contains articles on many of the points above.*

### Software and code

Policy information about [availability of computer code](#)

Data collection

No software was used for data collection.

Data analysis

Prism 6 was used for for statistical analysis. Optimouse ver. 3.0 and Synapse ver. 94 was used for data analysis.

For manuscripts utilizing custom algorithms or software that are central to the research but not yet described in published literature, software must be made available to editors/reviewers. We strongly encourage code deposition in a community repository (e.g. GitHub). See the Nature Research [guidelines for submitting code & software](#) for further information.

### Data

Policy information about [availability of data](#)

All manuscripts must include a [data availability statement](#). This statement should provide the following information, where applicable:

- Accession codes, unique identifiers, or web links for publicly available datasets
- A list of figures that have associated raw data
- A description of any restrictions on data availability

Statistical analysis was performed using datapoints reported in Figures. Primary datapoints are provided directly in figures and are additionally provided in a Supplemental Excel file (Supplemental Source Data).

### Field-specific reporting

Please select the one below that is the best fit for your research. If you are not sure, read the appropriate sections before making your selection.

- ☒ Life sciences ☐ Behavioural & social sciences ☐ Ecological, evolutionary & environmental sciences

# Life sciences study design

All studies must disclose on these points even when the disclosure is negative.

Sample size	Sample sizes were based on prior expertise and publications, and are disclosed in each figure legend.
Data exclusions	Data from mice that did not investigate both odor sources in the two-choice odor test were excluded from analysis, as they were not effectively making a comparison/choice. This was extremely rare, and the exclusion criteria were pre-established and are described in the methods.
Replication	Experiments in Figures 1b, 1d, 3b, 3e, Extended Figure 1b, 1d, 1e, 2b, 3b, 3c, 7b, 7c, 7f, 7g, and 10d were reproduced and verified in equal cohorts of male and female mice. Images in Extended Data Figure 9 were representative of 3 independent biological replicates involving different mice.
Randomization	Mice were randomly assigned to control groups or experimental groups, with comparisons kept age-matched and sex-matched.
Blinding	Data analysis was performed blinded to test animal identity, including test animal genotype and prior experimental manipulations.

# Reporting for specific materials, systems and methods

We require information from authors about some types of materials, experimental systems and methods used in many studies. Here, indicate whether each material, system or method listed is relevant to your study. If you are not sure if a list item applies to your research, read the appropriate section before selecting a response.

Materials & experimental systems		Methods	
n/a	Involved in the study	n/a	Involved in the study
<input type="checkbox"/>	<input checked="" type="checkbox"/> Antibodies	<input checked="" type="checkbox"/>	<input type="checkbox"/> ChIP-seq
<input type="checkbox"/>	<input checked="" type="checkbox"/> Eukaryotic cell lines	<input checked="" type="checkbox"/>	<input type="checkbox"/> Flow cytometry
<input checked="" type="checkbox"/>	<input type="checkbox"/> Palaeontology	<input checked="" type="checkbox"/>	<input type="checkbox"/> MRI-based neuroimaging
<input type="checkbox"/>	<input checked="" type="checkbox"/> Animals and other organisms		
<input checked="" type="checkbox"/>	<input type="checkbox"/> Human research participants		
<input checked="" type="checkbox"/>	<input type="checkbox"/> Clinical data		

## Antibodies

Antibodies used	AGRP: Neuromics, GT15023, goat, lot401818; NPY: Peninsula Laboratories, T-4070.0050, rabbit, lotA15692; donkey anti goat alexa 568: Thermo Fisher Scientific, A11507, lot371957; donkey anti rabbit alexa 647: Jackson ImmunoResearch, 711-605-152, lot 142730, horseradish peroxidase conjugated anti-Digoxigenin antibody: Roche Applied Science, 11207733910, lot35698000, TSA-plus Cyanine 3: PerkinElmer, NEL744001KT, lot2574097
Validation	We selected antibodies that were validated in previous publications. Furthermore, NPY antibodies were validated by loss of signal in NPY knockout mice, while AGRP antibodies were validated based on a characteristic and specific staining pattern in the arcuate nucleus.

## Eukaryotic cell lines

Policy information about [cell lines](#)

Cell line source(s)	HEK293T from ATCC
Authentication	Purchased from manufacturer. The cell lines were not further authenticated.
Mycoplasma contamination	The cell lines were not tested for mycoplasma contamination.
Commonly misidentified lines (See <a href="#">ICLAC</a> register)	No commonly misidentified cell lines were used in the study.

## Animals and other organisms

Policy information about [studies involving animals](#); [ARRIVE guidelines](#) recommended for reporting animal research

Laboratory animals	Animals were maintained under constant temperature (23 ± 1°C) and humidity (46 ± 5 %rh) with a 12-h light/dark cycle. Mice
--------------------	--

Laboratory animals	were used in this study, with strain/sex/age listed in the text, including wild type C57BL/6, Agrp-ires-Cre, loxP-ChR2, loxPHalorhodopsin, Mc4r-KO, Vgat-flox, Npy-KO, Npy1r-KO and Npy5r-KO. Male and female mice >8 weeks old were used.
Wild animals	The study did not include wild animals.
Field-collected samples	The study did not involve samples collected from the field.
Ethics oversight	All animal procedures followed the ethical guidelines outlined in the NIH Guide for the Care and Use of Laboratory Animals, and all protocols were approved by the institutional animal care and use committee (IACUC) at Harvard Medical School.

Note that full information on the approval of the study protocol must also be provided in the manuscript.